

Systematics in virial mass estimators for pressure-supported systems

Raphaël Errani^{1*}, Jorge Peñarrubia¹ & Matthew G. Walker²

¹ *Institute for Astronomy, University of Edinburgh, Royal Observatory, Blackford Hill, Edinburgh EH9 3HJ, UK*

² *McWilliams Center for Cosmology, Department of Physics, 5000 Forbes Ave., Carnegie Mellon University, Pittsburgh, PA 15213, USA*

May 1 2018

ABSTRACT

Mass estimators are a key tool to infer the distribution of dark matter in pressure-supported systems like dwarf spheroidal galaxies (dSphs). We construct an estimator for enclosed masses based on the virial theorem which is insensitive to anisotropy in the velocity dispersion and tailored to yield masses with minimum uncertainty introduced by our ignorance on (i) the shape of the inner halo profile, and (ii) how deeply the stellar component is embedded within the halo: $M(< 1.8R_h) \approx 3.5 \times 1.8R_h \langle \sigma_{\text{los}}^2 \rangle G^{-1}$, where by R_h we denote the projected half-light radius and by $\langle \sigma_{\text{los}}^2 \rangle$ the luminosity-averaged squared line-of-sight velocity dispersion. Tests against controlled simulations show that this method provides unbiased mass estimates with an accuracy of ~ 10 per cent. Application to published kinematic data of Milky Way dSphs reveals a tight correlation between enclosed mass and luminosity. Using N -body models we show that tidal stripping has little effect on this relation. Comparison against cuspy and cored dark matter haloes extracted from controlled re-simulations of the Aquarius A2 merger tree show that the high mass densities of ultra-faint galaxies are not compatible with large dark matter cores, and that the (total) halo masses of the Milky Way dSphs span a remarkably narrow range ($8 \lesssim \lg(M/M_\odot) \lesssim 10$) at present, showing no clear trend with either galaxy size or luminosity.

Key words: Local Group, galaxies: kinematics and dynamics, galaxies: dwarf, dark matter

1 INTRODUCTION

Understanding the distribution of dark matter (DM) on galactic scales is at the root of constraining DM particle properties and processes of baryonic feedback. Dwarf spheroidal galaxies (dSphs), lying at the faintest end of the galaxy luminosity function and reaching mass-to-light ratios of up to $\sim 10^3$ (see e.g. Walker et al. 2007; McConnachie 2012) are promising candidates to study the DM distribution on kpc scales. But obtaining such constraints through kinematic data is a challenging task: the galaxies are observed in projection, and precise velocity measurements are feasible only along the line of sight - though recently attempts have been made to constrain the 3D motion of stars in the Sculptor dwarf galaxy (Massari et al. 2018).

Having access only to velocities along the line of sight, the enclosed mass $M(< r_0)$ within a specific radius r_0 may be obtained from the projected virial theorem for spherical systems (see e.g. Merrifield & Kent 1990; Agnello & Evans 2012), relating the projected components of the pressure and potential energy tensors, $2K_{\text{los}} = -W_{\text{los}}$:

$$\langle \sigma_{\text{los}}^2 \rangle = \frac{4\pi G}{3} \int_0^\infty r v_\star(r) M(< r) dr, \quad (1)$$

where by $\langle \sigma_{\text{los}}^2 \rangle$ we denote the luminosity-averaged squared line-

of-sight velocity dispersion, and by $v_\star(r)$ the stellar tracer density profile. For the case of self-gravitating systems, Merritt (1987) describes how to infer $M(< r_0)$ from measurements of $\langle \sigma_{\text{los}}^2 \rangle$ under the assumption of a specific spherical mass profile. Building on this approach, for the case of a stellar tracer population embedded in a DM halo,

$$M(< r_0) = \frac{3}{4\pi G} \langle \sigma_{\text{los}}^2 \rangle \left[\int_0^\infty r v_\star(r) \tilde{M}(< r) dr \right]^{-1}, \quad (2)$$

where by $\tilde{M}(< r) \equiv M(< r)/M(< r_0)$ we denote the spherical mass profile normalised by the mass enclosed within some radius r_0 . This method is based entirely on projected and averaged dispersion measurements (and extending it to include tangential velocity components is straightforward, see section 6), but has the disadvantage of having to specify the normalised mass profile $\tilde{M}(< r)$ in advance. For the specific case of dwarf galaxies embedded in DM haloes, this means making assumptions on the DM halo shape and on how deeply the stellar component is embedded within the halo.

Alternatively, masses enclosed within a deprojected radius r_0 can be obtained from the radial velocity dispersion $\sigma_r(r)$ measured at a radius $r = r_0$ by means of the Jeans' equations (see e.g. Binney & Tremaine 1987),

$$M(< r_0) = \frac{r_0 \sigma_r^2(r_0)}{G} \left(\frac{d \ln v_\star(r_0)}{d \ln r} + \frac{d \ln \sigma_r^2(r_0)}{d \ln r} + 2\beta(r_0) \right), \quad (3)$$

where $\beta(r) \equiv 1 - \sigma_\perp^2(r)/\sigma_r^2(r)$ parametrises the anisotropy of the

* E-mail: raer@roe.ac.uk

velocity dispersion as a function of spherical radius r , $\sigma_{\perp}^2(r)$ being the tangential component of the velocity dispersion. The observed line-of-sight velocity dispersion $\sigma_{\text{los}}(R)$ measured at a projected radius R on the other hand is related to the radial velocity dispersion $\sigma_r(r)$ and anisotropy parameter $\beta(r)$ through (see e.g. [Binney & Mamon 1982](#)):

$$\sigma_{\text{los}}^2(R) = \frac{2}{\Sigma_*(R)} \int_R^{\infty} \left[1 - \frac{R^2}{r^2} \beta(r) \right] \frac{v_* \sigma_r^2(r)}{\sqrt{r^2 - R^2}} dr, \quad (4)$$

where $\Sigma_*(R)$ is the surface brightness at radius R . The above two equations do not yield a unique solution for $M(< r_0)$ without making further assumptions on the mass profile $M(< r)$ and on $\beta(r)$. For example, for the case of isotropic ($\beta = 0$) King models embedded in [Navarro et al. \(1997\)](#) haloes, [Peñarrubia et al. \(2008a\)](#) show that measuring the mass $M(< r_0)$ enclosed within the projected King core radius $r_0 = R_c$ minimises the uncertainty introduced by how deeply the stellar component is segregated within the DM halo. Their estimator reads $M(< R_c) \approx 1.44 R_c \sigma_{\text{los}}^2(0) G^{-1}$, where $\sigma_{\text{los}}^2(0)$ denotes the central line-of-sight velocity dispersion.

Current galaxy formation models do not yield clear predictions for the behaviour of $\beta(r)$. In principle, $\beta(r)$ does not need to be a monotonic function of r , and it might vary between different stellar populations within the same dwarf. Various methods have been proposed to avoid the mass - anisotropy degeneracy arising from our ignorance of $\beta(r)$. One approach are mass estimators constructed under the assumption that the enclosed mass is directly proportional to the observed line-of-sight velocity dispersion:

$$M(< r_0) \propto r_0 G^{-1} \langle \sigma_{\text{los}}^2 \rangle. \quad (5)$$

[Walker et al. \(2009\)](#) model the stellar tracer profiles as Plummer spheres and assume flat velocity dispersion profiles to estimate the enclosed mass as $M(< R_h) \approx 2.5 R_h \langle \sigma_{\text{los}}^2 \rangle G^{-1}$, showing numerically that the uncertainty introduced by a constant β is relatively small when measuring the enclosed mass at the projected half-light radius R_h . [Wolf et al. \(2010\)](#) reach a similar conclusion by analytical means, showing that the deprojected half-light radius approximately coincides with the radius where the anisotropy parameter $\beta(r)$ (modelled using a three-parameter function) has the smallest effect on the inferred enclosed mass. Their estimator reads $M(< r_h) \approx 3.0 r_h \langle \sigma_{\text{los}}^2 \rangle G^{-1}$, where $r_h \approx 4/3 R_h$ is the deprojected half-light radius. For the family of Michie-King distribution functions, [Amorisco & Evans \(2012\)](#) find that $M(< 1.7 R_h) \approx 5.8 R_h \sigma_{\text{los}}^2(R_h) G^{-1}$, where $\sigma_{\text{los}}^2(R_h)$ is measured at the half-light radius. By purely numerical means, [Campbell et al. \(2016\)](#) find $M(< 1.8 R_h) \approx 6.0 R_h \langle \sigma_{\text{los}}^2(< 1.04 R_h) \rangle G^{-1}$ from a dispersion-supported sample of galaxies of the APOSTLE simulation project ([Sawala et al. 2016](#)), averaging σ_{los}^2 within $1.04 R_h$. Mass estimators in the form of equation 5 have been tested on cosmological simulations ([Campbell et al. 2016](#); [González-Samaniego et al. 2017](#)) and proven to give accurate masses within a factor of unity.

The mass - anisotropy degeneracy may be broken if kinematic measurements of several chemo-dynamically distinguishable stellar populations within the same dSph can be obtained as discussed e.g. by [Saglia et al. \(2000\)](#), [Battaglia et al. \(2008\)](#) and [Amorisco & Evans \(2012\)](#), whereas [Diakogiannis et al. \(2014\)](#) suggest to measure σ_{los} at different radii and to model $\beta(r)$ using splines. With access to proper motions tangentially to the line of sight for a subsample of tracer stars, stronger constraints on $\beta(r)$ can be obtained (see e.g. [Strigari et al. 2007](#); [Watkins et al. 2013](#)). [Łokas & Mamon \(2003\)](#) show that a joint analysis of the velocity dispersion profile and higher order moments like the kurtosis may be used to break the mass - anisotropy degeneracy under specific assumptions for

the form of $\beta(r)$. [Breddels et al. \(2013\)](#) model dSphs by Schwarzschild orbit superposition to fit both the observed light distribution as well as the second and fourth order velocity moments, and apply the method to a catalogue of 2000 stars of the Sculptor dSph. They show that with 2000 tracers, the central slope Γ can't be constrained to tell cuspy from cored profiles, and $\beta(r)$ can't be constrained for radii smaller than 0.1 kpc - these authors conclude that to obtain unbiased estimates of Γ , a larger number of tracer stars is necessary. [Richardson & Fairbairn \(2014\)](#) use virial shape parameters derived from the fourth order virial equations to constrain DM density profiles compatible with the observed kinematics of embedded stellar tracers. Applied to the Sculptor dSph, the authors find that a cuspy DM halo is favoured if the stellar distribution is modelled as a Plummer profile. If the outer slope of the stellar profile however is allowed to vary, the available kinematic data does not allow to constrain the central DM profile slope. Using N -body mock data, [Read & Steger \(2017\)](#) show that with 10^4 tracer stars, no reliable $\beta(r)$ profile can be recovered from projected velocities and Jeans analysis alone. However, making use also of virial shape parameters or velocity measurements tangentially to the line of sight, using 10^3 tracer stars, both $\beta(r)$ and the underlying mass profile can be constrained within a few multiples of the half-light radius. A different approach is discussed by [Wang et al. \(2015\)](#), who fit analytical distribution functions to observables extracted from stellar tracers embedded in DM haloes of the Aquarius ([Springel et al. 2008](#)) simulations. These authors find that the derived halo masses are biased (by up to 40 per cent) even when using not only line-of-sight but also tangential velocity measurements.

Mass estimators in the form of equation 5 played a crucial role in identifying possible tensions between N -body simulations of Milky Way-like DM haloes, and the observed population of satellite galaxies of the Milky Way: [Boylan-Kolchin et al. \(2011\)](#) made use of the [Wolf et al. \(2010\)](#) estimator to identify N -body subhaloes compatible with the mean densities of Milky Way dwarfs, finding that none of the bright Milky Way dwarfs are dense enough to be embedded in haloes similar to the most massive simulated N -body subhaloes of the Aquarius simulations (the *too big to fail problem*). Based on estimates of enclosed masses of two distinct stellar populations embedded in the same DM halo, [Walker & Peñarrubia \(2011\)](#) introduced a method to determine the slope $\Gamma = \Delta \ln M / \Delta \ln r$ of the underlying DM halo, finding that both the Fornax and the Sculptor dSph must be embedded in DM haloes with constant-density cores, in conflict with the centrally divergent density cusps of haloes in DM-only simulations (the *cusp/core problem*). [Laporte et al. \(2013\)](#) subsequently showed that also for triaxial DM haloes, the [Walker & Peñarrubia \(2011\)](#) method gives reliable lower limits on the slope Γ . [Sawala et al. \(2015\)](#) use halo masses derived by [Peñarrubia et al. \(2008a\)](#) for Milky Way dSphs using the [Walker et al. \(2009\)](#) estimator to motivate their corrections to stellar mass - halo mass relations obtained from abundance matching based on DM-only simulations.

More recently, [Fattahi et al. \(2018\)](#) make use of the [Wolf et al. \(2010\)](#) estimator to study the tidal evolution DM haloes of the APOSTLE simulations compatible with the observed kinematics of Milky Way dSphs.

The use of the projected spherical virial theorem has several advantages over Jeans analysis for the construction of mass estimators of the form of equation 5: The virial theorem does not contain any functional dependence on $\beta(r)$ and thereby avoids the mass-anisotropy degeneracy. Also systematic biases of inferred enclosed masses and slopes Γ follow directly from the assumptions made on the DM and stellar density profiles and are independent of sample

size. Furthermore, the average squared dispersion $\langle \sigma_{\text{los}}^2 \rangle$ is a sum over all stars and does not require any binning of data. This makes mass estimators of the form of equation 5 based on the virial theorem applicable also to systems with only few stellar tracers - carefully factoring in the uncertainties due to sample size on the measured squared velocity dispersion as pointed out by Laporte et al. (2018).

In this contribution, we study a virial mass estimator which is minimally affected by our ignorance on two key parameters: (i) the shape of the inner DM halo profile, and (ii) the spatial segregation of the stellar tracers within the DM halo. In section 2 we introduce the spherical virial theorem and discuss the systematics of mass estimators for dwarf galaxies consisting of a stellar tracer population embedded inside a DM halo. In section 3 we construct a mass estimator which is tailored to minimise the uncertainty introduced by our ignorance on the central slope of the underlying DM profile as well as on how deeply embedded the stellar component is within the DM halo. We do test this mass estimator on a catalogue of N -body mocks. Section 4 discusses how to obtain the total halo masses of dwarf galaxies, breaking the degeneracy between structural parameters constrained by use of the virial theorem with the help of controlled cosmological simulations. In section 5, we estimate the masses of Milky Way dwarf galaxies using the methods introduced in the previous sections, and discuss implications of the derived stellar mass - halo mass relation for satellite galaxies. Section 6 summarises methods and main results.

2 MASS ESTIMATES FROM THE VIRIAL THEOREM

With the aim of estimating masses of dwarf galaxies from their observed velocity dispersions while avoiding the infamous mass - anisotropy degeneracy, in the spirit of Agnello & Evans (2012), we construct a mass estimator based on the projected virial theorem for spherical systems,

$$2K_{\text{los}} + W_{\text{los}} = 0. \quad (6)$$

We distinguish between the mass profile $M(< r)$ which sources the potential, and a mass-less tracer component of density $v_*(r)$ embedded in this potential. The pressure term is given by the projected velocity dispersion of the tracer and can be measured directly:

$$2K_{\text{los}} = 2\pi \int_0^\infty \Sigma_*(R) \sigma_{\text{los}}^2(R) R dR \equiv \langle \sigma_{\text{los}}^2 \rangle, \quad (7)$$

where by Σ_* and σ_{los}^2 we denote the surface density and line-of-sight velocity dispersion of the tracer, respectively. The potential energy term

$$W_{\text{los}} = -\frac{4\pi G}{3} \int_0^\infty r v_*(r) M(< r) dr \quad (8)$$

can be calculated for a given tracer density profile v_* and mass distribution $M(< r)$. Equations 6 - 8 allow $\langle \sigma_{\text{los}}^2 \rangle = -W_{\text{los}}$ to be calculated from the tracer and mass profiles alone. In contrast to the Jeans' equations, these virial equations and in specific the integral $\langle \sigma_{\text{los}}^2 \rangle$ are independent of anisotropies in the tracer velocity dispersion and thereby avoid the mass - anisotropy degeneracy.

The mass within a radius r_0 can be computed from the observed $\langle \sigma_{\text{los}}^2 \rangle$ as $M(< r_0) = \mu r_0 \langle \sigma_{\text{los}}^2 \rangle / G$ where

$$\mu(r_0) = -\frac{G M(< r_0)}{r_0 W_{\text{los}}} \quad (9)$$

is a dimensionless function of the radius r_0 and the parameters describing the tracer density and mass distribution.

2.1 Self-gravitating systems

As a first example, let us consider the case of a spherical system where the tracer density equals the mass density. For Dehnen (1993) profiles of total mass M_{tot} , scale radius a , scale density $\rho_s = (3 - \gamma)M_{\text{tot}}/4\pi a^3$, outer slope $\beta = 4$ and central slope γ , written in terms of the general $\{\alpha, \beta, \gamma\}$ profile with $\alpha = 1$,

$$\rho(r) = \rho_s \left(\frac{r}{r_s}\right)^{-\gamma} \left[1 + \left(\frac{r}{r_s}\right)^\alpha\right]^{(\gamma-\beta)/\alpha}, \quad (10)$$

the potential energy term becomes

$$W_{\text{los}} = -\frac{GM_{\text{tot}}}{a} \frac{1}{6(5-2\gamma)} \quad (11)$$

and

$$\mu_\gamma(r_0/a) = \left(1 + \frac{a}{r_0}\right)^{\gamma-3} \left(\frac{a}{r_0}\right) 6(5-2\gamma) \quad (12)$$

is a function of the radius r_0 and the scale radius a in the combination r_0/a alone. For a fixed r_0 , μ_γ reduces to a number, e.g. for the half-mass radius $r_{1/2} = a/(2^{1/(3-\gamma)} - 1)$, $\mu_1(r_{1/2}) = 9(\sqrt{2} - 1) \approx 3.7$ and $\mu_0(r_{1/2}) = 15(2^{2/3} - 2^{1/3}) \approx 4.9$.

2.2 Stellar tracer embedded in DM potential

For the case of dwarf galaxies with a stellar population embedded inside a DM halo, the mass profile which sources the potential is not accessible to direct observation. Let us assume that the projected half-light radius R_h and the luminosity-averaged squared velocity dispersion $\langle \sigma_{\text{los}}^2 \rangle$ are known quantities. This motivates a virial mass estimator for the enclosed mass $M(< r_0)$ with $r_0 = \lambda R_h$ of the form (Amorisco & Evans 2012):

$$M_{\text{est}}(< \lambda R_h) = \frac{\mu \lambda R_h \langle \sigma_{\text{los}}^2 \rangle}{G}, \quad (13)$$

where λ and μ are dimensionless factors.

Using equation 13, we now aim to determine the mass enclosed within the spherical radius $r_0 = \lambda R_h$. We treat stars as mass-less tracers of the underlying DM potential, consequently $M(< r)$ is determined by the DM profile alone. In the following, we assume that the stellar tracer distribution follows a spherical Plummer profile, $\{\alpha_*, \beta_*, \gamma_*\} = \{2, 5, 0\}$. To develop some intuition for the range of values which μ can take, let's consider a (scale-free) power-law DM profile with $\rho \propto r^{-\gamma}$, i.e. the asymptotic case $R_h/r_{\text{max}} \rightarrow 0$ of a stellar population deeply embedded inside the DM host halo. Then μ is a function of λ and γ alone,

$$\mu_\gamma(\lambda) \stackrel{R_h \rightarrow 0}{=} \frac{2\lambda^{2-\gamma}}{B(\gamma/2, (5-\gamma)/2)} \quad (14)$$

where by B we denote the Euler beta function. For $\gamma = 1$ this reduces to $\mu_1 = 3\lambda/2$, whereas for $\gamma \rightarrow 0$, $\mu_\gamma \rightarrow 0$ as $\langle \sigma_{\text{los}}^2 \rangle = -W_{\text{los}}$ diverges.

For non scale-free DM haloes, e.g. the density profile of equation 10 with scale radius a and two different asymptotic behaviours for $r \gg a$ and $r \ll a$, μ is not only a function of λ but also of the segregation parameter R_h/r_{max} describing how deeply embedded the stars are within the DM halo. There, by r_{max} we denote the radius of maximum circular velocity $v_{\text{max}} = (GM(< r_{\text{max}})/r_{\text{max}})^{1/2}$. Motivated by the result of controlled simulations that DM haloes undergoing tidal stripping have steeper outer slopes than field haloes, i.e. $\beta \approx 5$ (see Peñarrubia et al. 2009, 2010) in contrast to the outer slope of $\beta = 3$ of NFW profiles (Navarro et al. 1997),

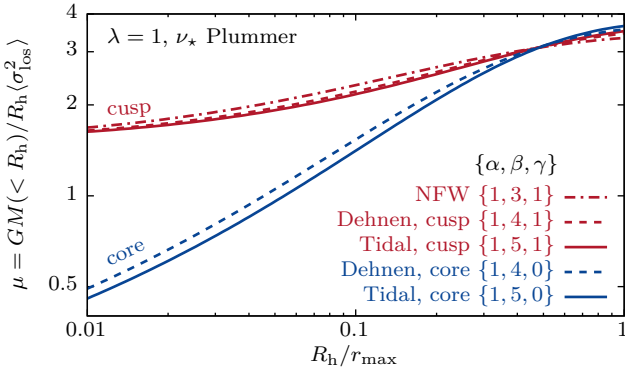


Figure 1. Dimensionless factor μ for $\lambda = 1$ (equation 13) as a function of segregation R_h/r_{\max} for stellar Plummer profiles with projected half-light radius R_h embedded in cored ($\gamma = 0$) and cuspy ($\gamma = 1$) DM haloes for tidally stripped systems, $\{\alpha, \beta, \gamma\} = \{1, 5, \gamma\}$ (see equation 10). For comparison, the functional dependence of μ on segregation is also shown for cuspy and cored Dehnen ($\beta = 4$) and NFW ($\beta = 3$) profiles.

Fig. 1 shows μ for the choice of $\lambda = 1$ as a function of the segregation parameter R_h/r_{\max} for stellar Plummer spheres embedded in cored ($\gamma = 0$) and cuspy ($\gamma = 1$) DM haloes with density profile as in equation 10, using $\beta = 5$ and $\rho_s = M_{\text{tot}}(3 - \gamma)(4 - \gamma)/4\pi a^3$. We choose $\alpha = 1$ motivated by the value found for equilibrium haloes in cosmological N -body simulations (Navarro et al. 1997). For comparison, the functional behaviour of μ is also shown for Dehnen, i.e. $\{\alpha, \beta, \gamma\} = \{1, 4, \gamma\}$, and NFW $\{1, 3, 1\}$ profiles. In the limit $R_h/r_{\max} \rightarrow 0$, we recover the asymptotic behaviour of equation 14 for $\lambda = 1$: $\mu \rightarrow 3/2$ for haloes with $\gamma = 1$, and $\mu \rightarrow 0$ for cored ones. For the segregations shown, μ is less sensitive to the steepness of the outer slope ($\beta = 3, 4, 5$) of the DM halo than it is to the inner one ($\gamma = 0, 1$).

Our ignorance of R_h/r_{\max} limits us to the use of a constant value of μ when estimating masses using equation 13. This leads to a systematic uncertainty on the estimated masses, and this uncertainty is more pronounced for cored haloes where μ diverges for the case of deeply embedded stellar populations. In section 3 we will discuss choices of μ, λ which minimise this uncertainty.

2.3 Slope estimates from two stellar populations

If we do have at hand two chemo-dynamically distinguishable stellar populations with projected half-light radii $R_{h,\text{inner}}, R_{h,\text{outer}}$ (where $R_{h,\text{inner}} < R_{h,\text{outer}}$) embedded in the same DM halo, the combined mass estimates derived from both populations can be used to infer the slope Γ of the underlying DM profile:

$$\Gamma = \frac{d \ln M(< r)}{d \ln r} \approx \underbrace{\frac{\Delta \ln \mu}{\Delta \ln R_h}}_{\varepsilon} + 1 + \underbrace{\frac{2 \ln \sigma_{\text{outer}} / \sigma_{\text{inner}}}{\ln R_{h,\text{outer}} / R_{h,\text{inner}}}}_{\text{WP11}}, \quad (15)$$

where WP11 refers to the estimator introduced by Walker & Peñarrubia (2011) under the assumption of constant μ , and writing for brevity $\sigma \equiv \langle \sigma_{\text{los}}^2 \rangle^{1/2}$. We will now explore how ε depends on the stellar tracer density profile v_* . For this aim, we embed two stellar tracer populations with projected half-light radii $R_{h,\text{inner}}$ and $R_{h,\text{outer}} = 2R_{h,\text{inner}}$ in cuspy ($\gamma = 1$) or cored ($\gamma = 0$) tidally stripped DM haloes (equation 10 with $\alpha = 1, \beta = 5$). The top panel of Fig. 2 shows the resulting ε as a function of segregation:

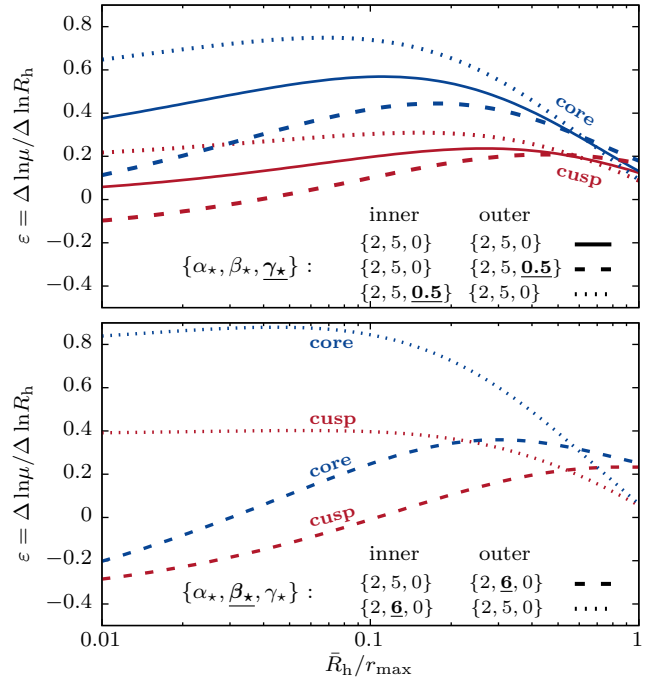


Figure 2. Logarithmic slope $\varepsilon = \Delta \ln \mu / \Delta \ln R_h$ computed for two stellar tracer populations with half-light radii $R_{h,\text{inner}}$ and $R_{h,\text{outer}} = 2R_{h,\text{inner}}$, embedded in cuspy ($\gamma = 1$) or cored ($\gamma = 0$) DM haloes with $\{\alpha, \beta, \gamma\} = \{1, 5, \gamma\}$ density profile (equation 10). The slope is shown as a function of the mean half-light radius $\bar{R}_h = (R_{h,\text{inner}} + R_{h,\text{outer}})/2$. *Top panel:* solid lines show ε for systems where both the inner and the outer stellar populations have Plummer $\{\alpha_*, \beta_*, \gamma_*\} = \{2, 5, 0\}$ density profiles. The dashed curves correspond to systems where one of the tracer populations has a shallow central density cusp of slope γ_* . *Bottom panel:* the outer slope β_* of one of the tracers is chosen to be steeper than the Plummer case.

- If $v_{*,\text{inner}}$ and $v_{*,\text{outer}}$ are Plummer profiles, $\{\alpha_*, \beta_*, \gamma_*\} = \{2, 5, 0\}$, (solid lines), then $\varepsilon > 0$ for the range of segregations R_h/r_{\max} shown, i.e. in this case WP11 underestimates the slope Γ of the underlying DM profile with $\varepsilon \lesssim 0.2, 0.6$ for the cuspy and cored DM halo respectively.

- WP11 also underestimates Γ if the inner population has a shallow central density cusp, $\{\alpha_*, \beta_*, \gamma_*\} = \{2, 5, 0.5\}$, and the outer population follows a Plummer density profile (dotted lines).

- If instead the outer population has a shallow central density cusp and the inner population is a Plummer profile, then $\varepsilon < 0$ for cuspy haloes and segregations $R_h/r_{\max} \lesssim 0.1$, i.e. in this configuration, WP11 overestimates Γ (dashed lines).

In the bottom panel of Fig. 2, the outer slope of one of the stellar tracers is chosen to be steeper, $\{\alpha_*, \beta_*, \gamma_*\} = \{2, 6, 0\}$, than in the Plummer case:

- If the outer population has a steeper outer slope β_* whereas the inner population is a Plummer profile, then $\varepsilon < 0$ for deeply embedded tracers (dashed lines).

- On the other hand, if the inner population has a steeper outer slope and the outer population is a Plummer profile, ε takes values of up to order of unity for deeply embedded tracers in cored DM haloes (dotted lines).

These results show that the shapes of the stellar tracer profiles need

to be taken into account when estimating Γ , as omitting to do so may lead to under-estimation of Γ by values of up to order of unity.

3 UNBIASED MINIMUM VARIANCE MASS ESTIMATES

In the previous section, we have shown how our ignorance on the segregation parameter R_h/r_{\max} leads to an uncertainty on the estimated masses which depends on the shape of the underlying DM profile. We now aim to determine values $\bar{\lambda}, \bar{\mu}$ so that the mass estimator of equation 13 is unbiased regarding (i) the DM profile shape (ii) how deeply embedded the stellar population is within the DM halo. By unbiased we intend not to make prior assumptions about the specific value of the segregation parameter R_h/r_{\max} and the inner¹ slope γ of the DM potential. By minimum variance we intend to choose $\bar{\lambda}, \bar{\mu}$ so that the relative error on the estimated masses due to our ignorance on R_h/r_{\max} and γ is minimised.

3.1 Minimising the variance as a function of λ

Under the assumption of stellar Plummer spheres embedded in DM haloes of tidally stripped systems ($\alpha = 1, \beta = 5$ in equation 10), for a given value of λ , we marginalise μ (equation 13) over segregations in the range $0 \leq R_h/r_{\max} \leq 1$ and central DM slopes in the range $0 \leq \gamma \leq 1$:

$$\langle \mu(\lambda) \rangle = \int_0^1 d(R_h/r_{\max}) \int_0^1 d\gamma \mu_\gamma(\lambda, R_h/r_{\max}). \quad (16)$$

This marginalisation assumes flat distributions of R_h and r_{\max} . The upper limit of the integration range in R_h/r_{\max} is motivated by the findings reported in section 5.3 from a sample of Milky Way dwarf galaxies. For a relative error on the estimated masses of $\langle \mu/\bar{\mu} - 1 \rangle = 0$, we require $\bar{\mu} = \langle \mu(\lambda) \rangle$. Fig. 3 shows how $\langle \mu(\lambda) \rangle \pm s$ with $s^2 = \langle \mu(\lambda)^2 \rangle - \langle \mu(\lambda) \rangle^2$ evolves as a function of λ , as well as $\langle \mu_\gamma(\lambda) \rangle$ where we marginalise over R_h/r_{\max} alone, separately for cuspy ($\gamma = 1$) and cored ($\gamma = 0$) DM profiles. At λ_{eq} , there is no functional dependence on γ as $\langle \mu_{\gamma=0} \rangle = \langle \mu_{\gamma=1} \rangle \equiv \mu_{\text{eq}}$. For each DM profile, $\lambda_{\gamma, \text{min}}$ minimises the squared relative error s^2/μ^2 when marginalising over R_h/r_{\max} alone, whereas $\bar{\lambda} = 1.8, \bar{\mu} = 3.5$ minimises the squared relative error after marginalising over both γ and R_h/r_{\max} ². Table 1 lists the numerical values for μ, λ .

For $\bar{\mu}, \bar{\lambda}$ as above, our minimum variance estimator becomes:

$$M_{\text{est}}(< 1.8R_h) \approx 3.5 \times 1.8R_h G^{-1} \langle \sigma_{\text{los}}^2 \rangle. \quad (17)$$

This $\mu = \text{const}$ minimum variance estimator (equation 17) allows to constrain the enclosed mass $M(< 1.8R_h)$ with an uncertainty of $s/\bar{\mu} \approx 10$ per cent without making assumptions about the central slope of the underlying DM profile.

The numerical values of $\bar{\lambda}, \bar{\mu}$ depend on the choice of shape for the DM profile (in our case $\alpha = 1, \beta = 5$ and $0 \leq \gamma \leq 1$) and stellar profile (in our case Plummer spheres), as well as on the range of segregations R_h/r_{\max} and central slopes γ to marginalise over.

¹ As shown in Fig. 1, comparing the cuspy Dehnen profile with outer slope $\beta = 4$ to the NFW profile ($\beta = 3$), for deeply embedded stellar systems, the outer slope of the DM halo does not affect the value of μ by much

² The value $\bar{\mu} = \langle \mu^2 \rangle / \langle \mu \rangle$ minimises the squared relative error with $\langle (\mu/\bar{\mu} - 1)^2 \rangle = s^2/\langle \mu^2 \rangle < s^2/\langle \mu \rangle^2 = \langle (\mu/\bar{\mu} - 1)^2 \rangle$, however for this choice of $\bar{\mu}$, the relative error equals $\langle \mu/\bar{\mu} - 1 \rangle = -s^2/\langle \mu^2 \rangle < 0$, i.e. the estimator which minimises the squared relative error is biased.

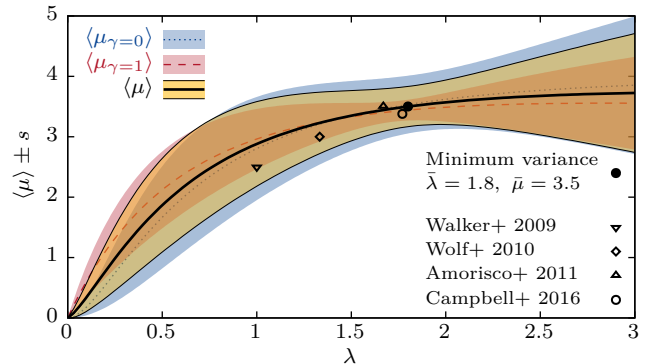


Figure 3. $\langle \mu_\gamma(\lambda) \rangle \pm s$ marginalised over segregation $0 \leq R_h/r_{\max} \leq 1$ as a function of λ for stellar Plummer spheres with projected half-light radius R_h embedded in cored ($\gamma = 0$, blue dotted curve and blue shaded area) and cuspy ($\gamma = 1$, red dashed curve and red shaded area) $\{\alpha, \beta, \gamma\} = \{1, 5, \gamma\}$ DM profiles (equation 10). The black curve and yellow shaded area show $\langle \mu \rangle \pm s$ marginalised not only over segregation, but also over $0 < \gamma < 1$. The values $\bar{\lambda}, \bar{\mu}$ for our minimum variance estimator are indicated by a filled circle, whereas literature values for λ, μ are plotted using open symbols.

Table 1. Numerical values for λ and μ of equation 13. $\bar{\lambda}$ minimises the squared relative error s^2/μ^2 when marginalising both over R_h/r_{\max} and γ (equation 16). When marginalising instead only over R_h/r_{\max} , then $\lambda_{\gamma, \text{min}}$ minimises the squared relative error for a given γ , whereas for $\lambda_{\text{eq}}, \langle \mu_{\gamma=0} \rangle = \langle \mu_{\gamma=1} \rangle \equiv \mu_{\text{eq}}$.

	$\bar{\lambda}$	$\bar{\mu}$	$\pm s$	λ_{eq}	μ_{eq}	$\pm s_\gamma$	$\bar{\lambda}_\gamma$	$\bar{\mu}_\gamma$	$\pm s_\gamma$
$\gamma = 0$						0.61	1.88	3.57	0.48
$\gamma = 1$	1.83	3.51	0.33	1.43	3.30	0.26	1.75	3.42	0.17

Other studies have found similar values for λ, μ using conceptually different approaches: Walker et al. (2009) use Jeans analysis to motivate the choice of $\lambda = 1, \mu = 5/2$ under the assumption of isotropy and a constant projected velocity dispersion. Wolf et al. (2010) use Jeans analysis to estimate the mass enclosed within the 3D half-light radius using the approximation $r_h = 4/3R_h$, which translates to $\lambda = 4/3, \mu \approx 3$. Amorisco & Evans (2011, 2012) use a distribution-function approach to determine $\lambda \approx 1.67, \mu \approx 3.50$ for Michie-King models, measuring σ_{os}^2 at the projected half-light radius. Campbell et al. (2016) find $\lambda \approx 1.77, \mu \approx 3.38$ empirically from a dispersion-supported sample of galaxies of the APOSTLE simulation project (Sawala et al. 2016), averaging σ_{los}^2 within $1.04R_h$.

3.2 Method comparison using N -body models

In the following, we will test the minimum variance estimator on a suite of N -body models taken from the controlled cosmological simulations introduced in Errani et al. (2017)³. This suite of N -body models consists of re-simulations of the accretion of all

³ In contrast to the set-up used in Errani et al. (2017), we use 10^7 N -body particles per satellite, the spatial resolution of the highest-resolving grid of the particle mesh code equals $r_{\max}/128$, and the Miyamoto & Nagai (1975) galactic disc has mass and scales evolving with redshift as in Bullock & Johnston (2005), with $M = 0.025M_{200}, a = 3.5 \text{ kpc}, b = 0.3 \text{ kpc}$ at $z = 0$, where by M_{200} we denote the virial mass of the Aquarius Aq-A2 main halo, and by a, b the horizontal and vertical disc scale lengths, respectively.

subhaloes with $M > 10^8 M_\odot$ of the Aq-A2 merger tree (Springel et al. 2008) onto an evolving, analytical Milky Way-like host potential consisting of an NFW halo and an axisymmetric disc. Subhaloes are modelled as equilibrium N -body realisations of either cuspy or cored Dehnen profiles with 10^7 particles and injected in the host potential at z_{infall} , defined by the peak of their mass evolution. All subhaloes are re-simulated with the same number of N -body particles independent of their mass, and the spatial resolution of the particle-mesh code is chosen as a function of the scale radius of each subhalo. This re-simulation technique allows us to follow the dynamical evolution of accreted substructures with the same numerical resolution for systems spanning many orders of magnitude in mass and size, and limits the impact of artificial disruption as discussed by van den Bosch et al. (2018). The subhaloes of the Aquarius simulation are cuspy, and have mass distributions before accretion consistent with the Navarro et al. (1997) profile. We generate our cuspy and cored Dehnen equilibrium subhaloes keeping M_{200} as given by the Aquarius simulation. We obtain r_{-2} (i.e. the radius where $d \ln \rho / d \ln r = -2$), which coincides with the NFW scale radius, from M_{200} using the median Prada et al. (2012) relation, and generate Dehnen models with that value of r_{-2} . We model the evolution of the stellar populations under the assumption that they are collision-less and mass-less systems which only trace the underlying DM potential by assigning mass-to-light ratios to each N -body particle at infall, following the approach of Bullock & Johnston (2005). At $z = 0$, average observational properties of the stellar population, e.g. the velocity dispersion, can be obtained from the DM N -body particles by applying the initially assigned mass-to-light ratios as weights. We consider all haloes which at $z = 0$ host a stellar population in virial equilibrium, requiring that $|2K + W| / (2K - W) < 0.2$ for the DM enclosed within r_{max} , and $|2K_{\text{los}} + W_{\text{los}}| / (2K_{\text{los}} - W_{\text{los}}) < 0.05$ for the stars. Masses and velocity dispersions are measured from these N -body haloes using bound particles only.

Fig. 4 shows the estimated enclosed masses $M(< \lambda R_h)$ of N -body models at $z = 0$ normalised by the true enclosed mass measured directly from the simulation as a function of segregation. The stellar population has a segregation of $R_{h,0}/r_{\text{max},0} = 1/10$ at infall, which increases due to tides, spreading at $z = 0$ over an interval $1/10 \lesssim R_h/r_{\text{max}} \lesssim 1$ for cuspy, and $1/10 \lesssim R_h/r_{\text{max}} \lesssim 1/2$ for cored systems. In the top panel, we compare our minimum variance estimator ($\mu = 3.5, \lambda = 1.8$) against the estimators of Walker et al. (2009) and Wolf et al. (2010) for cuspy DM haloes, whereas cored ones are plotted in the bottom panel. Dotted lines show the theoretical prediction of $M(< \lambda R_h)/M_{\lambda, \text{true}}$ from the virial theorem, i.e. $\mu_{\text{const}}/\mu(\lambda, R_h/r_{\text{max}})$. The estimated masses follow closely the predictions of the virial theorem, which leads us to the conclusion that the main uncertainty on the estimated masses for a given DM profile shape originates from our ignorance on how deeply embedded the stellar population is within the DM halo. For the range of segregations shown, when marginalising over the entire population of N -body mocks, the masses estimated from the minimum variance estimator are within ≈ 10 per cent of the true value. The other two estimators in question give a similar accuracy for cuspy systems. For cored systems, the Wolf et al. (2010) estimator over-estimates masses of cored systems by ≈ 20 per cent, whereas the Walker et al. (2009) estimator over-estimates the masses of cored systems by ≈ 50 per cent. The uncertainties we find when estimating masses of cored haloes using $\mu = \text{const}$ mass estimators are notably larger than the uncertainties described in Campbell et al. (2016), derived from the APOSTLE simulations (Sawala et al. 2016), and González-Samaniego et al. (2017), based on the FIRE

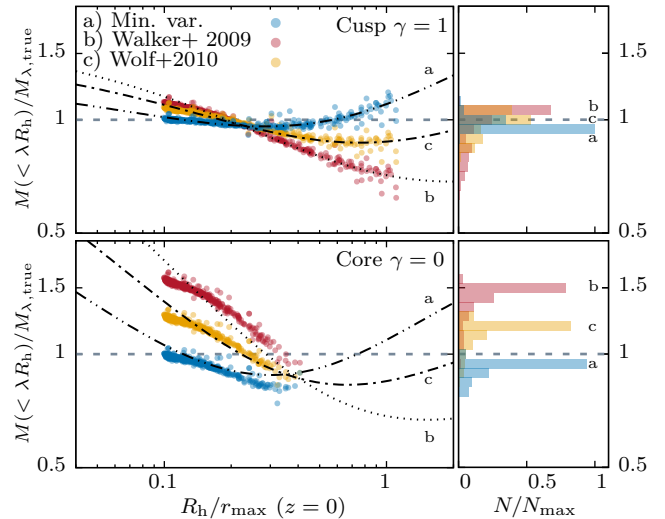


Figure 4. Estimated enclosed mass $M(< \lambda R_h)$ at $z = 0$ of N -body models taken from controlled re-simulations of the Aquarius A2 merger tree (see text), normalised by the true enclosed mass $M_{\lambda, \text{true}}$ measured directly from the simulation, as a function of segregation R_h/r_{max} . The embedded stellar tracers have a segregation of $R_{h,0}/r_{\text{max},0} = 1/10$ at infall. We compare our minimum variance estimator ($\mu = 3.5, \lambda = 1.8$) against the estimators of Walker et al. (2009) and Wolf et al. (2010) separately for cuspy (top panel) and cored (bottom panel) DM haloes. Dotted lines show the theoretical prediction of $M(< \lambda R_h)/M_{\lambda, \text{true}}$ from the virial theorem. The panels on the right are histograms obtained when summing over all haloes of the simulation.

simulations (Hopkins et al. 2014). This is due to the fact the N -body haloes in these simulations follow mass profiles close to the cuspy Navarro et al. (1997) profile (for FIRE, see also Chan et al. 2015, discussing the core sizes as function of halo mass), whereas our cored haloes have a large core size equal to the DM scale radius.

4 ESTIMATING THE (TOTAL) HALO MASS

In the previous sections, we focused on determining the mass enclosed within multiples of the half-light radius of dwarf galaxies embedded in DM haloes using $\mu = \text{const}$ mass estimators (equation 13). These estimators do not require to assume a specific DM profile when applying them to observational data - although the values of μ, λ can be motivated by a specific choice of profile, as done for the minimum-variance estimator, equation 17. We now focus on estimating the total halo mass from measurements of the stellar velocity dispersion (σ_{los}^2) and the half-light radius R_h .

For a DM halo density profile $\rho(r)$ with two free parameters, e.g. the total mass M_{tot} and a scale radius a for the profile of equation 10 with fixed $\{\alpha, \beta, \gamma\}$, the measurement of $\langle \sigma_{\text{los}}^2 \rangle$ and half-light radius R_h can be used to constrain one parameter as a function of the other, but is not sufficient to determine numerical values for both parameters simultaneously. Let us explore this degeneracy for the case of $\{\alpha, \beta, \gamma\} = \{1, 5, \gamma\}$ DM density profiles, i.e. DM profiles of tidally stripped systems, separately for the case of central DM cusps ($\gamma = 1$) and cores ($\gamma = 0$).

Extrapolating the enclosed mass: One way to obtain the degeneracy curve between the two halo structural parameters is to extrapolate the enclosed mass $M_{\text{est}}(< \lambda R_h) = \mu \lambda R_h \langle \sigma_{\text{los}}^2 \rangle / G$ estimated using a $\mu = \text{const}$ mass estimator. The cumulative mass profile cor-

responding to the density profile of equation 10 with $\alpha = 1, \beta = 5$ reads

$$M(< r/a, \gamma) = M_{\text{tot}} \left(\frac{r}{a} + 4 - \gamma \right) \left(\frac{r}{a} \right)^{3-\gamma} \left(\frac{r}{a} + 1 \right)^{\gamma-4}. \quad (18)$$

Defining $\tilde{M}(< r/a, \gamma) = M(< r/a, \gamma)/M_{\text{tot}}$, which is a function of the radius r and the scale radius a in the combination r/a alone, the total mass extrapolated from the enclosed mass $M_{\text{est}}(< \lambda R_h)$ then becomes

$$M_{\text{tot}}(R_h/a, \gamma) = M_{\text{est}}(< \lambda R_h/a) \tilde{M}^{-1}(< \lambda R_h/a, \gamma). \quad (19)$$

This total mass estimate is a function of the scale radius a of the DM halo, or equivalently of r_{max} , using

$$r_{\text{max}} = \frac{a}{2} \left(\sqrt{5\gamma^2 - 34\gamma + 57} + \gamma - 5 \right). \quad (20)$$

Equation 19 is defined for a specific DM profile shape and, for a given γ , can be written as a function of the segregation parameter R_h/r_{max} alone, but relies on a $\mu = \text{const}$ mass estimate originally constructed to avoid the segregation dependence and the choice of a DM profile shape in the first place. Moreover, equation 9 tells us how to calculate μ directly from the virial theorem as a function of the segregation parameter and the choice of DM profile. This motivates to estimate the total mass directly from the virial theorem.

Total mass from the virial theorem: Let's consider the projected potential energy term W_{los} of the spherical virial theorem, equation 6. This term can be computed for given density profiles of the DM halo and the stellar tracer population. For $\{\alpha, \beta, \gamma\} = \{1, 5, \gamma\}$ profiles with convergent total mass M_{tot} , we now define $\tilde{W}_{\text{los}}(\gamma, R_h/r_{\text{max}}) = W_{\text{los}}(M, \gamma, R_h/r_{\text{max}})/M_{\text{tot}}$, which does depend on the scale r_{max} and inner slope γ but not on the total mass M_{tot} of the DM halo. Then, using equation 6, we find

$$M_{\text{tot}}(R_h/r_{\text{max}}, \gamma) = -\langle \sigma_{\text{los}}^2 \rangle \tilde{W}_{\text{los}}^{-1}(\gamma, R_h/r_{\text{max}}). \quad (21)$$

For given observed values of $\langle \sigma_{\text{los}}^2 \rangle$ and R_h , and a choice of γ , the above equation for M_{tot} is a function of the segregation parameter R_h/r_{max} alone.

Degeneracy curves: To facilitate comparison with literature, this mass-segregation degeneracy can be cast as a one-dimensional degeneracy curve in the plane of the structural parameters $\{r_{\text{max}}, v_{\text{max}}\}$ of the DM halo, as first discussed by Peñarrubia et al. (2008a) for the case of stellar King profiles embedded in NFW haloes. For our case of tidally truncated systems with $\{\alpha, \beta, \gamma\} = \{1, 5, \gamma\}$ profiles, $v_{\text{max}} = [GM(< r_{\text{max}})/r_{\text{max}}]^{1/2}$ is calculated from equation 18 using for the total mass either equation 19 ($\mu = \text{const}$ extrapolation) or equation 21 (virial theorem). When including observational errors, this degeneracy curve becomes equivalent to what Agnello & Evans (2012) named *virial stripe*. Fig. 5 compares the $\{r_{\text{max}}, v_{\text{max}}\}$ curves obtained directly from the virial theorem to the ones based on extrapolated masses using the Walker et al. (2009) estimator, i.e. $\lambda = 1$ and using a constant $\mu = 5/2$ in equation 13. The curves are shown exemplarily for the Fornax dSph. For low (high) values of r_{max} , the virial theorem predicts larger (lower) values of v_{max} compatible with the same observed $\langle \sigma_{\text{los}}^2 \rangle$, R_h . For the range of r_{max} shown in Fig. 5, the difference in the compatible values of v_{max} for the Fornax dwarf between the Walker et al. (2009) and the virial theorem is less than a factor unity.

4.1 Breaking the degeneracy: halo parameters from controlled cosmological simulations

To constrain the location of a DM halo hosting an observed dwarf galaxy along the $\{r_{\text{max}}, v_{\text{max}}\}$ degeneracy curve determined by the

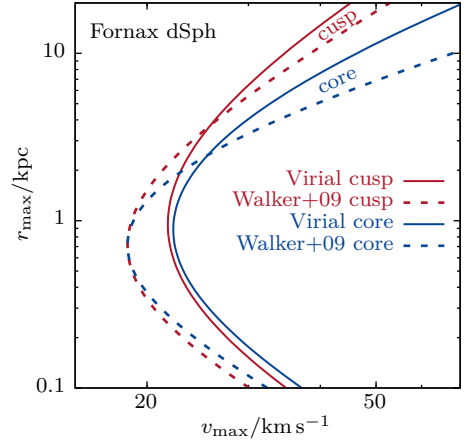


Figure 5. $\{r_{\text{max}}, v_{\text{max}}\}$ degeneracy curves for $\{\alpha, \beta, \gamma\} = \{1, 5, \gamma\}$ DM haloes compatible with the measurements of $\langle \sigma_{\text{los}}^2 \rangle$ and R_h of the Fornax dSph (from McConnachie 2012). Curves obtained directly from the virial theorem are compared to those based on mass estimates using the Walker et al. (2009) estimator, shown separately for cuspy ($\gamma = 1$) and cored ($\gamma = 0$) DM profiles.

measured values of $\langle \sigma_{\text{los}}^2 \rangle$ and R_h , we use the controlled cosmological simulations of the formation of Milky Way-like DM haloes discussed in section 3.2 to obtain the range of values $\{r_{\text{max}}, v_{\text{max}}\}$ take for haloes at $z = 0$. We infer the range of possible halo structural parameters of the dwarf galaxy by selecting those simulated DM haloes consistent with the $\{r_{\text{max}}, v_{\text{max}}\}$ degeneracy curve constrained by the observed kinematics of the dwarf. This approach of breaking the $\{r_{\text{max}}, v_{\text{max}}\}$ degeneracy is closely related to the method introduced by Peñarrubia et al. (2008a), where a cosmological $\{r_{\text{max}}, v_{\text{max}}\}$ relation for field haloes was used. Using a relation for field haloes neglects the effects of tidal stripping on the DM profiles as experienced by satellite galaxies like the Milky Way dSphs, which we do take into account by using $\{r_{\text{max}}, v_{\text{max}}\}$ values of simulated tidally stripped haloes. Fig. 6 shows the values of $\{r_{\text{max}}, v_{\text{max}}\}$ of the surviving population of simulated haloes at $z = 0$, separately for cuspy (left panel) and cored (right panel) models. We only consider simulated haloes where both the DM enclosed within r_{max} and the stars are approximately in virial equilibrium, requiring $|2K + W|/(2K - W) < 0.2$ for the DM, and $|2K_{\text{los}} + W_{\text{los}}|/(2K_{\text{los}} - W_{\text{los}}) < 0.05$ for the stars. When determining r_{max} and v_{max} of the N -body subhaloes, we consider bound particles only. The difference between cuspy and cored models becomes more pronounced with decreasing v_{max} . Cored models are more extended than their cuspy counterparts for $v_{\text{max}} \lesssim 20 \text{ km/s}$, and the relation shows substantially more scatter in the cored case. Also shown is the evolution of $\{r_{\text{max}}, v_{\text{max}}\}$ along *tidal tracks* (see appendix A) as a function of the fraction of remnant mass M_{max} enclosed within r_{max} with respect to the value at infall. Whereas cuspy systems evolve approximately along the initial $\{r_{\text{max}}, v_{\text{max}}\}$ relation, keeping the range of $\{r_{\text{max}}, v_{\text{max}}\}$ values rather narrow, cored systems evolve away from the initial relation, causing the larger observed scatter. While cored substructures are prone to disruption by tides, which explains the absence of systems with mass losses as high as for some cuspy models (see colour coding in Fig. 6), in this study, we do not match abundances of the simulated systems but structural parameters only, either by fitting the enclosed mass

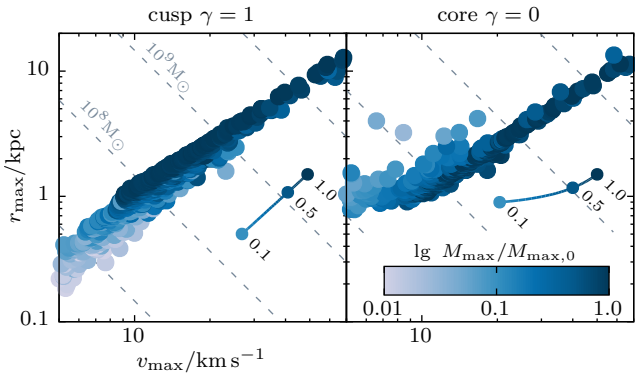


Figure 6. $\{r_{\max}, v_{\max}\}$ values of DM subhaloes at $z=0$ of our controlled re-simulations of the Aquarius A2 merger tree. We model the accreted subhaloes to have either cuspy (left panel) or a cored (right panel) density profiles. The colour coding shows the mass M_{\max} enclosed within r_{\max} at $z=0$ relative to the enclosed mass at infall. The solid curve and filled circles show the evolution within the $\{r_{\max}, v_{\max}\}$ plane along tidal evolutionary tracks (see appendix A), numbers denoting the fraction of remnant mass M_{\max} enclosed within r_{\max} .

$M(< \lambda R_h)$ using a $\mu = \text{const}$ mass estimators, or by fitting the observed velocity dispersion $\langle \sigma_{\text{los}}^2 \rangle$.

Fitting the enclosed mass $M(< \lambda R_h)$: When obtaining the $\{r_{\max}, v_{\max}\}$ degeneracy curve by extrapolating masses estimated through a $\mu = \text{const}$ mass estimator (see equation 19), it is a natural choice to break the degeneracy by selecting the simulated halo which matches best the estimated enclosed mass $M_{\text{est}}(< \lambda R_h)$ computed from the observed values of $\langle \sigma_{\text{los}}^2 \rangle$ and R_h . For each simulated halo, we measure $\{r_{\max}, v_{\max}\}$ and compute the mass $M_{\text{sim}}(< \lambda R_h)$ assuming an $\{\alpha, \beta, \gamma\} = \{1, 5, \gamma\}$ profile with structural parameters $\{r_{\max}, v_{\max}\}$. We then select the halo which minimises

$$\chi_{M(< \lambda R_h)}^2 = \left(M_{\text{est}}(< \lambda R_h) - M_{\text{sim}}(< \lambda R_h) \right)^2 / \text{var}, \quad (22)$$

where by var we denote the propagated variances from the observational uncertainties on $\langle \sigma_{\text{los}}^2 \rangle$ and R_h . The variance is estimated through Monte-Carlo runs assuming Gaussian errors on $\langle \sigma_{\text{los}}^2 \rangle$ and R_h to account for the correlation between $\text{var}(M_{\text{est}}(< \lambda R_h))$ and $\text{var}(M_{\text{sim}}(< \lambda R_h))$ introduced by the uncertainty in R_h .

Fitting the velocity dispersion $\langle \sigma_{\text{los}}^2 \rangle$: When obtaining the degeneracy curve directly from the virial theorem (equation 21), for each simulated halo with structural parameters $\{r_{\max}, v_{\max}\}$, we calculate the expected velocity dispersion $\langle \sigma_{\text{los, sim}}^2 \rangle$ from the virial theorem, using the observed value of R_h ,

$$\langle \sigma_{\text{los, sim}}^2 \rangle = -W_{\text{los}} = \frac{4\pi G}{3} \int_0^\infty r v_*(r) M(< r) dr. \quad (23)$$

In the above equation, $v_*(r)$ is the density profile of a Plummer sphere, $\{\alpha_*, \beta_*, \gamma_*\} = \{2, 5, 0\}$, with projected half-light radius R_h , and $M(< r)$ is the cumulative mass profile for an $\{\alpha, \beta, \gamma\} = \{1, 5, \gamma\}$ DM halo with structural parameters $\{r_{\max}, v_{\max}\}$. We then confront this expected velocity dispersion $\langle \sigma_{\text{los, sim}}^2 \rangle$ to the observed velocity dispersion $\langle \sigma_{\text{los}}^2 \rangle$ by computing

$$\chi_{\langle \sigma_{\text{los}}^2 \rangle}^2 = \left(\langle \sigma_{\text{los}}^2 \rangle - \langle \sigma_{\text{los, sim}}^2 \rangle \right)^2 / \text{var}. \quad (24)$$

The variance term in the denominator is again obtained by Monte-Carlo sampling, assuming Gaussian errors on the observables R_h and $\langle \sigma_{\text{los}}^2 \rangle$.

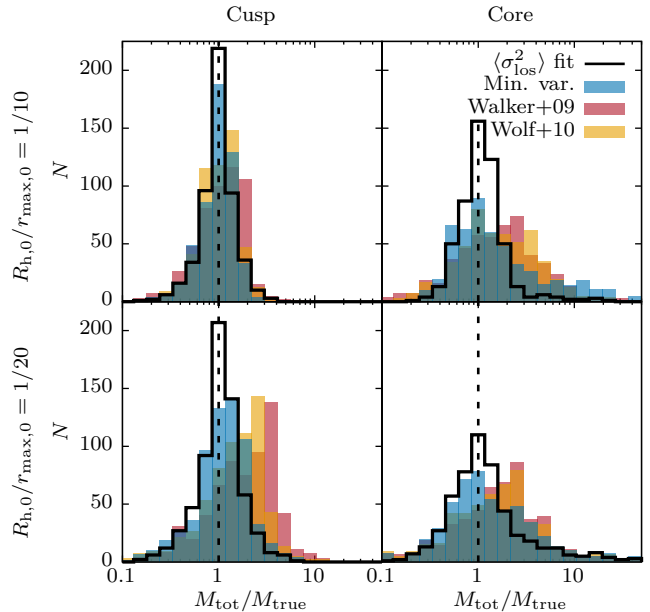


Figure 7. Histograms of estimated over true total halo mass $M_{\text{tot}}/M_{\text{true}}$ for four different catalogues of N -body subhaloes obtained from re-simulations of the Aquarius A2 merger tree: cuspy (cored) models are shown in the left (right) column, and the embedded stellar populations have an initial segregation of $R_{h,0}/r_{\max,0} = 1/10$ ($1/20$) in the top row (bottom row). For each catalogue of N -body subhaloes, four different methods are used to estimate the total halo mass: direct fits of $\langle \sigma_{\text{los}}^2 \rangle$ (see equation 23), as well as masses extrapolated from three $\mu = \text{const}$ estimators, including the minimum variance estimator introduced in section 3.

4.2 Test of self-consistency using N -body models

Before applying the mass estimator to kinematic data of Milky Way dwarf galaxies in section 5.3, as a consistency check we recover the masses of the catalogue of N -body subhaloes described in section 3.2, i.e. we embed stellar populations in the same DM subhaloes which we use to break the $\{r_{\max}, v_{\max}\}$ degeneracy. In Fig. 7 we compare the masses estimated through direct $\langle \sigma_{\text{los}}^2 \rangle$ fits to masses extrapolated from $\mu = \text{const}$ estimators, assuming DM profiles with $\alpha = 1$ and $\beta = 5$ (see equation 10). The logarithms of the masses obtained from the virial estimator (black lines) are distributed approximately symmetrically around the true mass with $\langle \lg M/M_{\text{true}} \rangle = 0.0 \pm 0.2$ for cuspy systems, and 0.0 ± 0.2 (0.1 ± 0.5) for cored systems with an initial segregation of $R_{h,0}/r_{\max,0} = 1/10$ ($1/20$).

On average, masses extrapolated from the three $\mu = \text{const}$ estimators are over-estimated, i.e. $\langle \lg M/M_{\text{true}} \rangle > 0$ for all four subhalo catalogues. For masses extrapolated for cuspy systems from the minimum variance $\mu = \text{const}$ estimator introduced in section 3 we find $\langle \lg M/M_{\text{true}} \rangle \sim 0.0 \pm 0.3$, and $\lesssim 0.2 \pm 0.5$ for cored systems, i.e. bias and spread of the distribution are larger than for the masses obtained directly from the virial theorem. The bias $\langle \lg M/M_{\text{true}} \rangle$ is larger for the other two $\mu = \text{const}$ estimators. For systems with an initial segregation of $1/20$, both the Walker et al. (2009) and the Wolf et al. (2010) estimator give $\langle \lg M/M_{\text{true}} \rangle = 0.2 \pm 0.3$ (0.2 ± 0.6) for cuspy (cored) systems. Overall, we find larger biases and spreads in the distribution of recovered masses for cored systems than for cuspy ones. Cored systems do lose mass to tides more easily than cuspy systems, and their mass pro-

files show more extra-tidal features, i.e. the our assumption of $\{\alpha, \beta, \gamma\} = \{1, 5, 0\}$ profiles does not match cored systems well which have lost large fractions of their initial mass.

5 DISCUSSION: THE HALO MASSES OF MILKY WAY DWARF SPHEROIDAL GALAXIES

We apply the minimum variance mass estimator to observational data of Milky Way dwarf galaxies compiled by [McConnachie \(2012\)](#), supplemented with data by [Adén et al. \(2009\)](#) (for Hercules) and [Torrealba et al. \(2016\)](#); [Caldwell et al. \(2017\)](#) (for Crater 2) to infer the structural properties of DM haloes compatible with the observed values of $\langle \sigma_{\text{los}}^2 \rangle$ and R_h . The velocity dispersions measured for Milky Way dSphs are often limited to one measurement per galaxy, e.g. the central velocity dispersion, or the velocity dispersion averaged within a certain radius, not necessarily up to infinity. Limited by the data available, for the following mass estimates we use the observed $\sigma_{\text{los,obs}}$ as listed in [McConnachie \(2012\)](#) and assume $\sigma_{\text{los,obs}}^2 = \langle \sigma_{\text{los}}^2 \rangle$ in the notation of equation 7.

5.1 The tight correlation of enclosed mass and luminosity

In this section we show that enclosed mass $M(< 1.8R_h)$ and luminosity L_* of Milky Way dSph galaxies are tightly correlated, and that the effect of the tidal field of the Milky Way is small for the evolution of this correlation since accretion of the dwarfs. To estimate the enclosed mass within $\bar{\lambda} = 1.8$ half-light radii R_h , we use the minimum-variance $\mu = \text{const}$ estimator (equation 17). Fig. 8 shows the tight correlation between L_* and $M(< 1.8R_h)$, and numerical values are listed in table 2. The faintest dwarfs of the sample with $L_* \sim 10^3 L_\odot$ have enclosed masses of $\sim 10^6 M_\odot$, whereas the Fornax and Sagittarius⁴ dwarf galaxies with $L_* \sim 10^7 L_\odot$ have enclosed masses of the order $\sim 10^8 M_\odot$. The mean mass-to-light ratios Υ_* averaged within the respective half-light radii therefore decrease with luminosity and span a range of $1 \lesssim \lg \Upsilon_* \lesssim 3$. This correlation has already been noted by [McConnachie \(2012\)](#), making use of the [Walker et al. \(2009\)](#) mass estimator and plotting masses enclosed within the half-light radius $M(< R_h)$ as a function of absolute V-band magnitude. Note that the luminosity L_* is not used in the inference of $M(< 1.8R_h)$, distinguishing this correlation from the relation between enclosed mass $M(< R_h)$ and half-light radius R_h discussed in [Walker et al. \(2009\)](#). The colour-coding of Fig. 8 shows the metallicity Fe/H of the dwarfs, which also increases with $M(< 1.8R_h)$.

Our results suggest that the correlation of $M(< 1.8R_h)$ and L_* is mainly driven by internal processes, i.e. star-formation and feedback, and that tides through by Milky Way halo do have little effect on the relation. Solid lines in Fig. 8 show the evolution of luminosity and enclosed mass along tidal evolutionary tracks (see appendix A), i.e. as a function of the remnant mass fraction $M_{\text{max}}/M_{\text{max},0}$, separately for the assumption of stellar populations embedded in cuspy and cored DM haloes. The initial segregation of the stellar populations is chosen to be $R_{h,0}/r_{\text{max},0} = 1/10$. dSphs evolving along these tidal tracks can lose up to two orders of magnitude of their mass M_{max} enclosed within r_{max} , or equivalently of their total

⁴ The Sagittarius dwarf galaxy is close to pericentre and perturbed by tidal forces of the Milky Way halo and disc (see e.g. [Peñarrubia et al. 2009](#); [Lokas et al. 2010](#)). Our mass estimates are derived under the assumption of virial equilibrium of the stellar tracer component, a requirement which is not guaranteed to hold for Sagittarius.

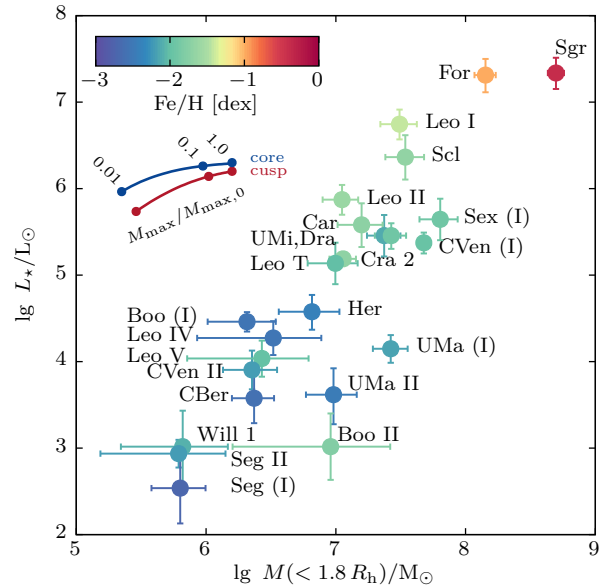


Figure 8. Luminosity L_* as a function of the mass $M(< 1.8R_h)$ enclosed within 1.8 half-light radii for Milky Way dwarf galaxies. Masses are estimated using the minimum-variance estimator (equation 17). The colour-coding shows metallicity Fe/H. Uncertainties are estimated by Monte Carlo sampling of symmetric Gaussian errors on $\langle \sigma_{\text{los}}^2 \rangle$ and R_h . The blue (red) solid curve shows the evolution along tidal tracks (see appendix A) for a stellar population with $R_{h,0}/r_{\text{max},0} = 1/10$ embedded in a cored (cuspy) DM profile, assuming $L_* \propto M_*$. Numerical values are listed in table 2.

mass under the assumption that the profile shape doesn't change, but experience a decrease in $M(< 1.8R_h)$ by only one order of magnitude. This is related to r_{max} decreasing during tidal stripping (see top panel of Fig. A1), which causes the mass enclosed within the central regions of the halo to decrease less rapidly than the total mass. As a consequence, the relation of luminosity and enclosed mass of Fig. 8 is not expected to broaden significantly during the tidal evolution of the dwarfs after accretion, and this holds both under the assumption of cuspy and cored DM halo profiles. However, internal processes like star formation will likely have an effect on the relation also after accretion, with star formation shown to be ongoing in some dSphs also after accretion - see e.g. [de Boer et al. \(2012\)](#), discussing that the latest star formation in the Fornax dwarf happened as recently as 250 Myrs ago.

5.2 Confronting measured densities and simulated haloes

When comparing the mean densities of ultra-faint Milky Way dwarfs to those of cored DM haloes taken from our re-simulations of the Aquarius A2 merger tree, we find that none of the simulated cored haloes are dense enough to host an ultra-faint dwarf. We compute the mean density, averaged within a spherical volume of radius $1.8R_h$, using the minimum variance mass estimator:

$$\langle \rho(< 1.8R_h) \rangle = M(< 1.8R_h)(4\pi/3)^{-1}(1.8R_h)^{-3}. \quad (25)$$

Fig. 9 shows the mean densities $\rho(< 1.8R_h)$ as a function of half-light radius R_h , as well as the mean density profiles of the cuspy ($\gamma = 1$) and cored ($\gamma = 0$) DM haloes of the controlled cosmological simulations of the formation of Milky Way-like haloes described in section 3.2. These profiles are obtained by fitting $\{r_{\text{max}}, v_{\text{max}}\}$ for each simulated DM halo at $z = 0$, and assuming an $\{\alpha, \beta, \gamma\} =$

Table 2. Structural parameters for the brightest Milky Way dSphs. Luminosity L_* , line-of-sight velocity dispersion σ_{los} and half-light radius R_h are taken from [McConnachie \(2012\)](#) - for Crater 2, L_* and R_h are then used to obtain the mean density $\rho_{1.8} \equiv \langle \rho(< 1.8R_h) \rangle$. Uncertainties on $M_{1.8}$ and $\rho_{1.8}$ are obtained by Monte Carlo sampling symmetric Gaussian errors on σ_{los} and R_h . Structural parameters of the DM haloes, i.e. r_{max} , v_{max} and total halo mass M_{tot} , are obtained by fitting the observed velocity dispersion σ to the N -body subhaloes of our re-simulations of the Aquarius A2 merger tree, as discussed in section 4. These quantities are listed separately for fits to N -body subhaloes with cuspy ($\gamma = 1$) and cored ($\gamma = 0$) DM profiles. Total halo masses of N -body subhaloes are extrapolated from the mass M_{max} enclosed within r_{max} under the assumption of density profiles for tidally stripped systems ($\alpha = 1$, $\beta = 5$ in equation 10). Uncertainties on r_{max} , v_{max} and M_{tot} indicate the range of values of those N -body subhaloes which satisfy $\chi^2 \leq \chi_{\text{min}}^2 + 1$.

	$\lg L_*/L_\odot$	$\sigma_{\text{los}}/\text{km s}^{-1}$	R_h/kpc	CUSP						CORE			
				$\lg \frac{M_{1.8}}{M_\odot}$	$\lg \rho_{1.8} \frac{\text{kpc}^3}{M_\odot}$	$v_{\text{max}}/\text{km s}^{-1}$	$r_{\text{max}}/\text{kpc}$	$\lg M_{\text{tot}}/M_\odot$	χ_{min}^2	$v_{\text{max}}/\text{km s}^{-1}$	$r_{\text{max}}/\text{kpc}$	$\lg M_{\text{tot}}/M_\odot$	χ_{min}^2
Sagittarius dSph	$7.34^{+0.18}_{-0.18}$	11.40 ± 0.70	2.62 ± 0.20	$8.70^{+0.06}_{-0.06}$	$6.06^{+0.09}_{-0.08}$	$21.76^{+1.35}_{-1.34}$	$2.02^{+1.12}_{-0.43}$	$8.82^{+0.21}_{-0.05}$	0.0	$21.51^{+1.45}_{-1.19}$	$2.94^{+0.21}_{-0.37}$	$8.89^{+0.09}_{-0.09}$	0.0
Fornax	$7.31^{+0.19}_{-0.20}$	11.70 ± 0.90	0.71 ± 0.08	$8.15^{+0.08}_{-0.08}$	$7.22^{+0.12}_{-0.11}$	$23.44^{+5.53}_{-1.99}$	$2.31^{+2.15}_{-0.72}$	$8.94^{+0.47}_{-0.18}$	0.0	$31.70^{+26.63}_{-4.05}$	$4.60^{+8.83}_{-0.61}$	$9.42^{+0.99}_{-0.18}$	0.0
Leo I	$6.74^{+0.17}_{-0.18}$	9.20 ± 1.40	0.25 ± 0.03	$7.49^{+0.13}_{-0.15}$	$7.91^{+0.15}_{-0.17}$	$27.90^{+11.86}_{-10.14}$	$3.70^{+3.07}_{-2.29}$	$9.29^{+0.57}_{-0.81}$	0.0	$65.01^{+8.59}_{-28.10}$	$10.72^{+3.71}_{-5.22}$	$10.41^{+0.24}_{-0.78}$	0.5
Sculptor	$6.36^{+0.25}_{-0.26}$	9.20 ± 1.40	0.28 ± 0.04	$7.54^{+0.14}_{-0.15}$	$7.81^{+0.19}_{-0.18}$	$27.20^{+4.87}_{-9.48}$	$3.94^{+1.07}_{-2.53}$	$9.30^{+0.25}_{-0.82}$	0.0	$65.01^{+8.59}_{-28.31}$	$10.72^{+3.71}_{-5.22}$	$10.41^{+0.24}_{-0.78}$	0.1
Leo II	$5.87^{+0.17}_{-0.18}$	6.60 ± 0.70	0.18 ± 0.04	$7.05^{+0.12}_{-0.15}$	$7.93^{+0.26}_{-0.21}$	$16.94^{+9.93}_{-4.19}$	$1.60^{+2.40}_{-0.69}$	$8.50^{+0.80}_{-0.49}$	0.0	$65.01^{+8.59}_{-46.78}$	$10.72^{+3.71}_{-9.10}$	$10.41^{+0.24}_{-1.93}$	0.1
Sextans (I)	$5.64^{+0.24}_{-0.24}$	7.90 ± 1.30	0.69 ± 0.04	$7.80^{+0.14}_{-0.16}$	$6.90^{+0.13}_{-0.17}$	$15.51^{+3.03}_{-3.48}$	$1.98^{+0.51}_{-1.06}$	$8.51^{+0.25}_{-0.52}$	0.0	$17.18^{+3.78}_{-4.58}$	$2.40^{+0.48}_{-1.15}$	$8.61^{+0.25}_{-0.53}$	0.0
Carina	$5.58^{+0.25}_{-0.26}$	6.60 ± 1.20	0.25 ± 0.04	$7.20^{+0.16}_{-0.18}$	$7.62^{+0.21}_{-0.20}$	$16.45^{+5.50}_{-6.46}$	$2.07^{+1.07}_{-1.56}$	$8.58^{+0.43}_{-1.04}$	0.0	$29.01^{+44.59}_{-16.04}$	$4.25^{+10.18}_{-3.00}$	$9.31^{+1.34}_{-1.23}$	0.0
Ursa Minor	$5.46^{+0.24}_{-0.24}$	9.50 ± 1.20	0.18 ± 0.03	$7.37^{+0.13}_{-0.13}$	$8.22^{+0.18}_{-0.16}$	$35.15^{+23.65}_{-12.04}$	$4.85^{+6.44}_{-3.26}$	$9.61^{+0.81}_{-0.85}$	0.0	$65.01^{+6.10}_{-16.74}$	$10.72^{+2.46}_{-3.08}$	$10.41^{+0.17}_{-0.41}$	4.0
Draco	$5.46^{+0.14}_{-0.15}$	9.10 ± 1.20	0.22 ± 0.02	$7.43^{+0.11}_{-0.13}$	$8.02^{+0.12}_{-0.14}$	$32.06^{+7.71}_{-11.92}$	$4.90^{+1.87}_{-3.31}$	$9.54^{+0.33}_{-0.80}$	0.0	$65.01^{+6.10}_{-16.74}$	$10.72^{+2.46}_{-3.08}$	$10.41^{+0.17}_{-0.41}$	1.6
Canes Venatici (I)	$5.37^{+0.12}_{-0.12}$	7.60 ± 0.40	0.56 ± 0.04	$7.68^{+0.05}_{-0.05}$	$7.04^{+0.07}_{-0.07}$	$15.27^{+1.12}_{-1.85}$	$1.86^{+0.29}_{-0.94}$	$8.47^{+0.12}_{-0.42}$	0.0	$17.07^{+1.36}_{-2.07}$	$2.18^{+0.49}_{-0.56}$	$8.56^{+0.15}_{-0.24}$	0.0
Crater 2	$5.19^{+0.04}_{-0.04}$	2.70 ± 0.30	1.07 ± 0.08	$7.06^{+0.10}_{-0.11}$	$5.59^{+0.11}_{-0.12}$	$5.93^{+0.57}_{-0.70}$	$0.39^{+0.04}_{-0.13}$	$6.98^{+0.09}_{-0.18}$	0.0	$5.20^{+1.38}_{-0.56}$	$0.92^{+3.08}_{-0.13}$	$7.15^{+0.84}_{-0.09}$	0.0
Leo T	$5.14^{+0.24}_{-0.24}$	7.50 ± 1.60	0.12 ± 0.01	$7.00^{+0.17}_{-0.21}$	$8.38^{+0.17}_{-0.23}$	$37.54^{+21.26}_{-22.36}$	$6.25^{+5.04}_{-5.10}$	$9.78^{+0.65}_{-1.52}$	0.0	$18.24^{+55.36}_{-5.26}$	$1.61^{+12.81}_{-0.36}$	$8.49^{+2.16}_{-0.41}$	1.9
Hercules	$4.58^{+0.19}_{-0.21}$	3.72 ± 0.91	0.33 ± 0.06	$6.82^{+0.21}_{-0.26}$	$6.89^{+0.27}_{-0.28}$	$6.90^{+1.97}_{-1.79}$	$0.41^{+0.50}_{-0.22}$	$7.12^{+0.57}_{-0.57}$	0.0	$8.13^{+8.54}_{-2.75}$	$1.15^{+3.03}_{-0.37}$	$7.64^{+1.18}_{-0.52}$	0.0
Bootes (I)	$4.46^{+0.11}_{-0.11}$	2.40 ± 0.70	0.24 ± 0.02	$6.32^{+0.22}_{-0.30}$	$6.78^{+0.22}_{-0.32}$	$4.40^{+1.30}_{-1.08}$	$0.20^{+0.21}_{-0.06}$	$6.42^{+0.52}_{-0.39}$	0.0	$5.68^{+2.77}_{-2.35}$	$1.11^{+2.89}_{-0.36}$	$7.31^{+0.81}_{-0.59}$	0.0
Leo IV	$4.27^{+0.19}_{-0.20}$	3.30 ± 1.70	0.21 ± 0.04	$6.52^{+0.37}_{-0.59}$	$7.20^{+0.41}_{-0.57}$	$6.37^{+4.85}_{-4.99}$	$0.52^{+0.81}_{-0.38}$	$7.16^{+0.90}_{-1.70}$	0.0	$10.15^{+8.16}_{-7.65}$	$1.81^{+2.37}_{-1.06}$	$8.03^{+0.79}_{-1.58}$	0.0
Ursa Major (I)	$4.15^{+0.16}_{-0.16}$	7.60 ± 1.00	0.32 ± 0.05	$7.42^{+0.13}_{-0.14}$	$7.54^{+0.18}_{-0.17}$	$16.42^{+7.07}_{-3.15}$	$1.53^{+2.00}_{-0.61}$	$8.45^{+0.67}_{-0.39}$	0.0	$24.65^{+48.95}_{-8.00}$	$3.11^{+11.31}_{-1.50}$	$9.03^{+1.62}_{-0.58}$	0.0
Leo V	$4.04^{+0.21}_{-0.21}$	3.70 ± 1.85	0.13 ± 0.03	$6.43^{+0.36}_{-0.58}$	$7.68^{+0.42}_{-0.60}$	$8.14^{+9.10}_{-6.76}$	$0.70^{+1.60}_{-0.56}$	$7.50^{+1.17}_{-2.04}$	0.0	$13.95^{+59.64}_{-11.45}$	$1.74^{+12.69}_{-0.98}$	$8.29^{+2.36}_{-1.83}$	0.0
Canes Venatici II	$3.90^{+0.22}_{-0.22}$	4.60 ± 1.00	0.07 ± 0.01	$6.35^{+0.19}_{-0.22}$	$8.37^{+0.25}_{-0.25}$	$18.21^{+10.76}_{-10.68}$	$2.22^{+2.24}_{-1.92}$	$8.70^{+0.71}_{-1.63}$	0.0	$18.24^{+52.88}_{-5.26}$	$1.61^{+11.56}_{-0.36}$	$8.49^{+2.09}_{-0.41}$	0.7
Ursa Major II	$3.62^{+0.31}_{-0.34}$	6.70 ± 1.40	0.15 ± 0.02	$6.98^{+0.18}_{-0.21}$	$8.10^{+0.21}_{-0.23}$	$23.71^{+8.36}_{-12.39}$	$3.34^{+1.68}_{-2.60}$	$9.11^{+0.44}_{-1.30}$	0.0	$65.01^{+8.59}_{-48.36}$	$10.72^{+3.71}_{-9.10}$	$10.41^{+0.24}_{-1.96}$	0.6
Coma Berenices	$3.58^{+0.27}_{-0.29}$	4.60 ± 0.80	0.08 ± 0.01	$6.37^{+0.15}_{-0.17}$	$8.35^{+0.18}_{-0.20}$	$17.23^{+9.65}_{-9.57}$	$1.99^{+2.02}_{-1.69}$	$8.61^{+0.69}_{-1.53}$	0.0	$18.24^{+49.16}_{-0.00}$	$1.61^{+9.72}_{-0.00}$	$8.49^{+1.98}_{-0.00}$	1.1
Bootes II	$3.02^{+0.38}_{-0.38}$	10.50 ± 7.40	0.05 ± 0.02	$6.96^{+0.46}_{-0.76}$	$9.49^{+0.54}_{-0.76}$	$63.03^{+7.08}_{-61.66}$	$8.91^{+5.34}_{-8.77}$	$10.38^{+0.30}_{-4.93}$	0.1	$18.24^{+55.36}_{-15.73}$	$1.61^{+12.81}_{-0.86}$	$8.49^{+2.16}_{-2.03}$	0.3
Willman 1	$3.02^{+0.42}_{-0.48}$	4.30 ± 1.80	0.03 ± 0.01	$5.82^{+0.35}_{-0.48}$	$9.25^{+0.40}_{-0.50}$	$58.80^{+11.31}_{-55.48}$	$11.29^{+2.96}_{-11.15}$	$10.43^{+0.25}_{-4.40}$	0.0	$18.24^{+55.36}_{-15.73}$	$1.61^{+12.81}_{-0.86}$	$8.49^{+2.16}_{-2.03}$	0.9
Segue II	$2.94^{+0.16}_{-0.16}$	3.40 ± 1.85	0.03 ± 0.00	$5.79^{+0.36}_{-0.60}$	$8.79^{+0.37}_{-0.61}$	$21.95^{+36.85}_{-20.57}$	$3.14^{+8.15}_{-3.00}$	$9.01^{+1.41}_{-3.56}$	0.0	$18.24^{+55.36}_{-15.73}$	$1.61^{+12.81}_{-0.86}$	$8.49^{+2.16}_{-2.03}$	0.3
Segue (I)	$2.54^{+0.39}_{-0.41}$	3.90 ± 0.80	0.03 ± 0.01	$5.80^{+0.20}_{-0.22}$	$9.04^{+0.27}_{-0.25}$	$37.54^{+21.26}_{-28.82}$	$6.25^{+5.04}_{-5.87}$	$9.78^{+0.65}_{-2.48}$	0.0	$18.24^{+49.16}_{-8.12}$	$1.61^{+9.72}_{-0.56}$	$8.49^{+1.98}_{-0.70}$	3.2

$\{1, 5, \gamma\}$ profile with the fitted values of $\{r_{\max}, v_{\max}\}$. Whereas for the re-simulation using cuspy subhaloes there are subhaloes with densities as high as the measured densities $\rho(< 1.8R_h)$ of Milky Way dwarfs, in the case of cored simulations, none of the simulated haloes is dense enough to be compatible with the ultra-faint galaxies in the sample (see right panel of Fig. 9). Fig. 9 also shows the evolution along tidal tracks (see appendix A) for a stellar population with an initial segregation of $R_{h,0}/r_{\max,0} = 1/10$, assuming $L_* \propto M_*$. With half-light radii staying near constant, the evolution of the mean density for cuspy systems reflects the previously discussed behaviour that a system being stripped two orders of magnitude of its total mass only loses one order of magnitude of its enclosed mass $M(< 1.8R_h)$, and therefore also $\rho(< 1.8R_h)$ drops by only one order of magnitude. The situation is notably different for dSphs embedded in cored DM haloes, which have half-light radii that expand during tidal stripping (see bottom panel of Fig. A1). For cored systems, losing two orders of magnitude of their total mass results in the average central density $\rho(< 1.8R_h)$ to drop by two orders of magnitude as well. As a consequence, if the ultra-faint galaxies of the sample did lose mass through tides previously, they must have been even denser in the past, rendering them even more incompatible with the cored DM haloes of our simulations⁵. This discrepancy is a consequence of our choice of the core size of the simulated haloes. The cored subhaloes injected in the evolving host potential are modelled as Dehnen (1993) density profiles with $\gamma = 0$, i.e. density profiles where the core size is equal to the scale radius, chosen to highlight the different tidal evolution of cored substructures compared to cuspy ones. Our findings suggest that the ultra faint dwarfs require core sizes that are much smaller than the dark matter scale radius.

5.3 (Total) halo mass - stellar mass relation

Extrapolating total halo masses from measured enclosed masses is an uncertain endeavour: whereas enclosed masses within multiples of the half-light radius are well constrained by measurements of $\langle \sigma_{\text{los}}^2 \rangle$ and R_h , constraints on the total halo mass are very weak ($\lambda \gg 1$ in Fig. 3). Total halo masses are therefore commonly extrapolated from enclosed masses under the assumption of median cosmological mass - concentration relations obtained for cuspy Navarro et al. (1997) profiles (see e.g. the discussion in Strigari et al. (2008), making use of the Bullock et al. (2001) relation between virial mass M_{vir} and v_{\max} derived using cosmological N -body simulations). Tidally stripped systems do have density profiles with steep outer slopes ($\beta \approx 5$, see Peñarrubia et al. 2009, 2010) and convergent total masses, in contrast to the Navarro et al. (1997) profile of field haloes with $\beta = 3$ and a divergent total mass. Adding to this, following the tidal evolution of low-mass subhaloes is a challenging task for traditional cosmological simulation with fixed N -body particle mass, and recent studies call for caution regarding

⁵ It is interesting to note that increasing the mass of the host halo will not ease the difference between the measured densities and those of cored simulated haloes: whereas for cuspy density profiles, those systems with the highest total mass also have the largest densities, this does not hold for cored haloes. For the case of tidally evolved, cored $\{\alpha, \beta, \gamma\} = \{1, 5, 0\}$ profiles, from equation 18 we find for the central density $\rho(0) = \rho_s \propto M_{\text{tot}}/a^3$. An empirical power-law fit to the relation between M_{tot} and the scale radius a , derived from the Aquarius A2 merger for systems with mass $\geq 10^8 M_{\odot}$, gives $a \propto M_{\text{tot}}^{0.4}$. Consequently for these mass scales, the central density decreases with mass.

numerical convergence of these simulations (van den Bosch et al. 2018).

We infer the total halo mass of Milky Way dwarf galaxies by fitting the observed line-of-sight velocity dispersion $\langle \sigma_{\text{los}}^2 \rangle$ to N -body DM subhaloes extracted from a re-simulation of the Aquarius A2 merger tree, as described in section 4. Fig. 10 shows $\{r_{\max}, v_{\max}\}$ degeneracy curves constrained by the measurements of velocity dispersion $\langle \sigma_{\text{los}}^2 \rangle$ and half-light radius R_h for Milky Way dSph galaxies assuming cuspy ($\gamma = 1$) or cored ($\gamma = 0$) DM density profiles for tidally stripped systems ($\alpha = 1, \beta = 5$ in equation 10). The $\{r_{\max}, v_{\max}\}$ values of N -body subhaloes at $z = 0$ of our controlled simulations are depicted by grey filled circles, and the haloes corresponding to the minimum- χ^2 estimates (see equation 24) are indicated using crosses. Table 2 lists the inferred masses and structural parameters for the minimum- χ^2 estimate. For the case of cored DM profiles, the dwarfs Ursa Minor and Segue (I) have $\chi_{\text{min}}^2 > 3$ and therefore result incompatible with all simulated subhaloes. Note that for cored systems, the $\{r_{\max}, v_{\max}\}$ degeneracy curves corresponding to ultra-faint galaxies do not intersect with any of the simulated cored DM haloes. Nevertheless the large observational uncertainties of the kinematics of these ultra-faint systems, for the case of cored DM profiles, we have $\chi_{\text{min}}^2 \gtrsim 0.3$ for all dwarfs with $L_* < 10^4 L_{\odot}$.

Based on the inferred total halo masses M_{tot} , we study the stellar- to halo mass relation of Milky Way satellite galaxies at $z = 0$. Using the rough approximation that $M_*/M_{\odot} \approx 1.5L_*/L_{\odot}$ (e.g. Martin et al. 2008), fig. 11 shows the stellar- and total halo masses. Halo masses inferred under the assumption of cuspy and cored subhaloes are shown in the top and bottom panels, respectively. Errorbars show the minimum and maximum masses of simulated subhaloes which satisfy $\chi^2 < \chi_{\text{min}}^2 + 1$. The stellar- to halo mass relations by Moster et al. (2010), Behroozi et al. (2013) and Sawala et al. (2016) are plotted using dashed grey lines, showing M_{200} as a proxy to the total halo mass (which for NFW, i.e. non tidally stripped profiles with $\beta = 3$, is diverging). For systems with $\lg L_*/L_{\odot} \gtrsim 5$, our findings are compatible with all three stellar- to halo mass relations shown. For the case of the Sagittarius and the Fornax dSphs, our inferred masses are smaller by one order of magnitude than the halo mass predictions for field haloes given the observed luminosities. In general, for the case of cuspy subhaloes, all classical Milky Way dSphs have inferred masses at the low-mass end of the abundance matching relations shown. This discrepancy is consistent with our understanding of the tidal evolution of dSph galaxies: when being accreted onto a larger galaxy, dSph galaxies initially lose predominantly DM and not stars, which are embedded deeply inside the galaxies' potential and are therefore less prone to stripping (Peñarrubia et al. 2008b). The tidal evolutionary tracks shown in Fig. 11 and discussed in appendix A show that dSphs with both cuspy and cored DM profiles can be stripped one order of magnitude of their dynamical mass due to tides while losing less than ten per cent of their stellar mass ($M_* \propto \Sigma_* R_h^2$). Note also that the correlation between luminosity and enclosed mass $M(< 1.8\lambda R_h)$ (see Fig. 8) is notably tighter than the correlation found between stellar mass and total halo mass. This also could be a consequence of the tidal evolution of the dwarfs: if at infall stellar mass and total halo mass were more tightly correlated, tides may have stripped significant fractions of DM but not of stars, as consistent with the tidal tracks for highly segregated stellar populations.

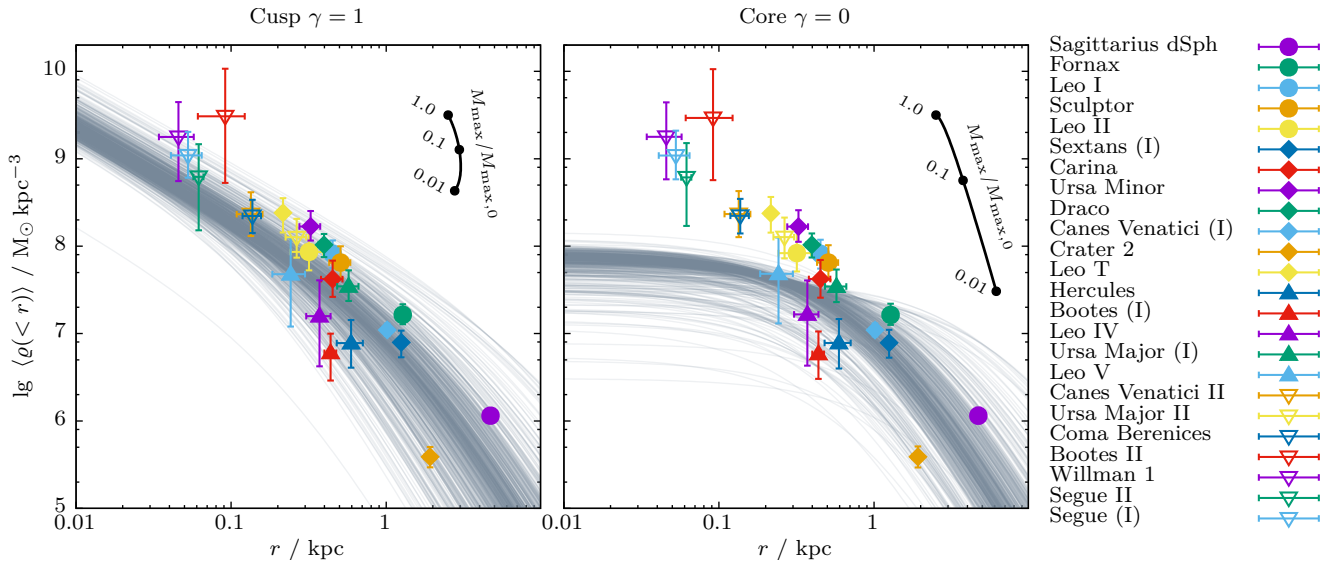


Figure 9. Mean densities $\rho(<1.8R_h)$ within 1.8 half-light radii R_h of Milky Way dSphs, estimated using the minimum-variance mass estimator (equation 17). Grey curves show the mean density profiles of cuspy ($\gamma = 1$, left panel) and cored ($\gamma = 0$, right panel) haloes of the controlled cosmological simulations introduced in section 3.2. These curves assume $\{\alpha, \beta, \gamma\} = \{1, 5, \gamma\}$ profiles with $\{r_{\max}, v_{\max}\}$ as fitted to the simulated haloes. Note that the ultra-faint Milky Way dwarfs are too dense to be compatible with any of the simulated cored DM haloes.

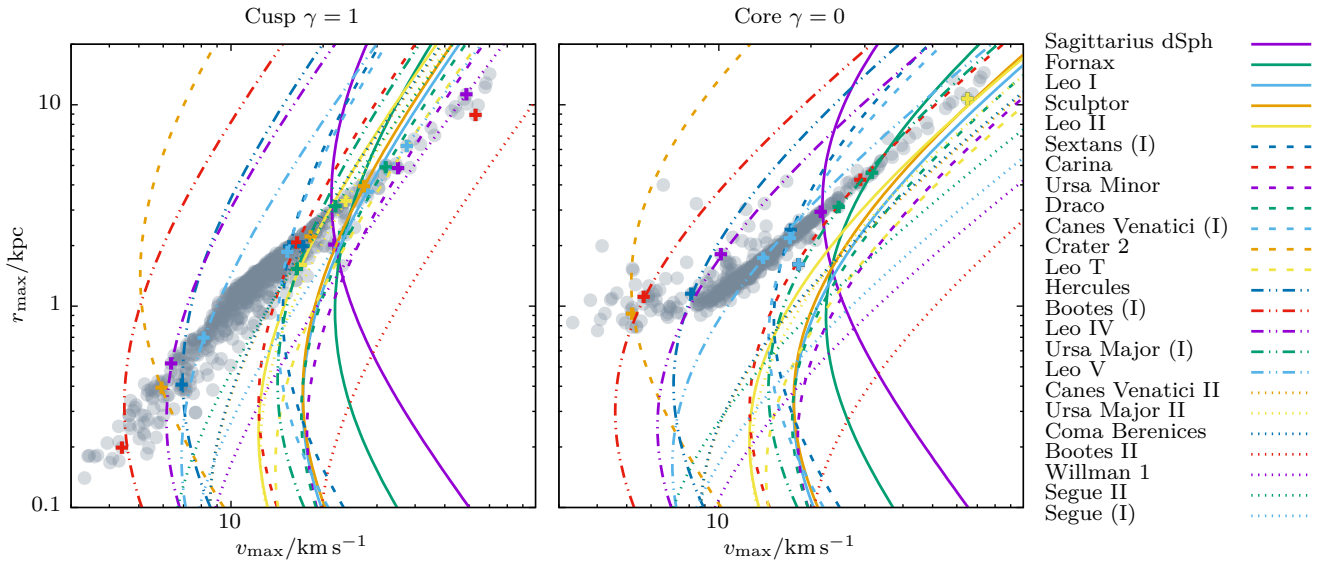


Figure 10. $\{r_{\max}, v_{\max}\}$ degeneracy curves of the DM haloes of Milky Way dSphs obtained by assuming cuspy (left panel, $\gamma = 1$) and cored (right panel, $\gamma = 0$) DM density profiles for tidally stripped systems ($\alpha = 1, \beta = 5$ in equation 10). $\{r_{\max}, v_{\max}\}$ values of subhaloes of our controlled cosmological simulations are shown by grey filled circles. Crosses indicate the minimum- χ^2 estimates (see equation 24). Note that the $\{r_{\max}, v_{\max}\}$ curves of the ultra-faint Milky Way dwarfs result incompatible with any of the simulated cored DM haloes.

5.4 Puzzling halo masses for ultra-faint dwarfs

For systems with $\lg L/L_{\odot} \lesssim 5$, we find an anti-correlation between stellar mass and halo mass, associating the faintest galaxies to the most massive haloes. For cored systems, Milky Way dwarf galaxies with luminosities spanning between $2 \lesssim L/L_{\odot} \lesssim 4$ are associated to

the DM haloes of mass of $\sim 10^9 M_{\odot}$, with an uncertainty of two orders of magnitude and $\chi^2_{\min} \gtrsim 0.3$. The corresponding $\{r_{\max}, v_{\max}\}$ degeneracy curves of Fig. 10 do not intersect with any $\{r_{\max}, v_{\max}\}$ value measured from the cored simulations. Note that dwarf galaxies evolving along the tidal tracks shown in Fig. 11 primarily lose

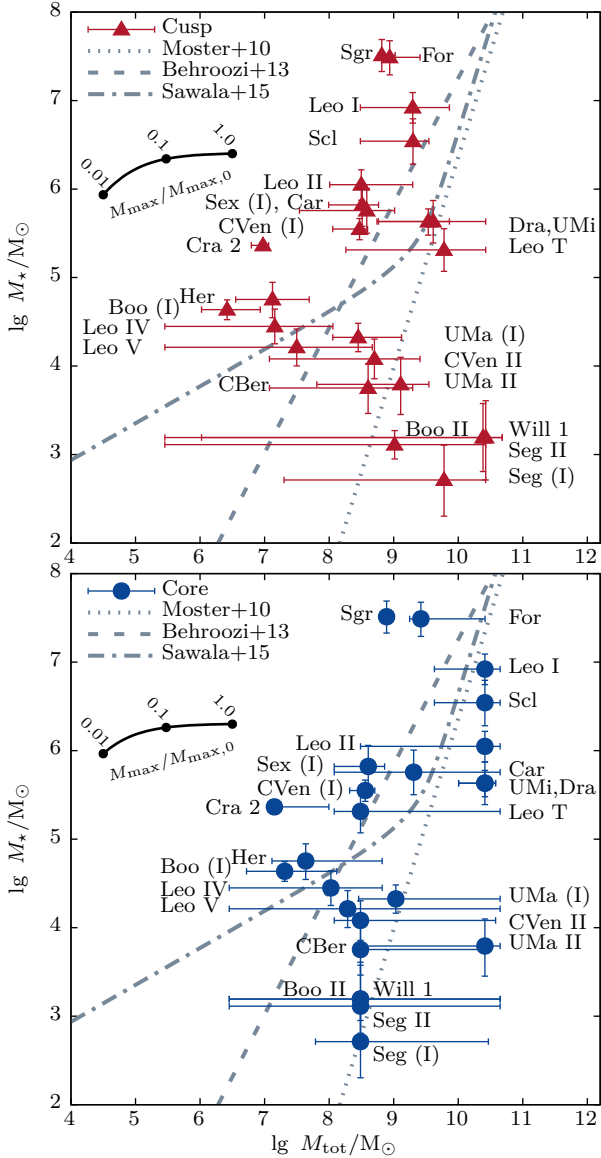


Figure 11. Stellar- and total halo masses inferred for Milky Way dwarf galaxies (McConnachie 2012) by fitting the observed velocity dispersion (σ_{los}^2) to the catalogue of subhaloes of our re-simulations of the Aquarius A2 merger tree. Abundance matching relations (Moster et al. 2010; Behroozi et al. 2013; Sawala et al. 2015) are shown as grey dashed lines. The back solid lines show the median evolution of M_* following the tidal tracks of Appendix A as a function of the fraction of remnant mass M_{max} enclosed within r_{max} .

DM and not stellar mass, and move away from the stellar mass-halo mass relation found for ultra-faints, i.e. tidal evolution cannot be at the origin of the observed anti-correlation.

There are however observational challenges which might be related to this counter-intuitive anti-correlation:

- Inflated masses might result from inflated velocity dispersion measurements: a striking example being the Hercules dSph, where Adén et al. (2009) found a reduction by roughly half from $7.33 \pm 1.08 \text{ km s}^{-1}$ to $3.72 \pm 0.91 \text{ km s}^{-1}$ after removing foreground contaminants.

- Similarly, peculiar velocities due to binary motion add to the observed velocity dispersion.

Furthermore, there are several systematic aspects of our method which call for caution.

- All our analysis is based on the virial theorem and thereby assumes dynamical equilibrium of the underlying stellar tracer component. Some dSphs do show extra-tidal (i.e. non-equilibrium) features, and the applicability of the virial theorem is then limited to the virialised core of the systems.

- We infer total halo masses of Milky Way dwarfs by selecting subhaloes extracted from simulations of Milky Way-like DM haloes compatible with the observed kinematics. For this purpose, we re-simulated a single merger tree of the Aquarius simulation. Cosmic variance will allow for a wider range of accretion scenarios, and possibly for a wider range of $\{r_{\text{max}}, v_{\text{max}}\}$ values at $z = 0$. This may increase the number of haloes compatible with the observed kinematics.

- The Aquarius A2 main halo has a virial mass of $1.84 \times 10^{12} M_{\odot}$, which is larger by a factor ~ 2 than estimates of the (total) Milky Way mass derived by use of the timing argument (Peñarrubia et al. 2016). Therefore also the simulated subhaloes, which we use to break the $\{r_{\text{max}}, v_{\text{max}}\}$ degeneracy of Milky Way dSphs, might have on average higher masses than Milky Way subhaloes.

- We infer masses separately under the assumption of cuspy and cored DM profiles, using a single choice of core size. Different core sizes are motivated by various physical models for core formation. Our choice to model the subhaloes at infall as Dehnen (1993) profiles with $\gamma = 0$ and $\gamma = 1$ are extreme cases, but as shown in Fig. 11, the impact of the assumed core size on the inferred total halo masses is relatively small.

In this contribution, we made use of measured velocity dispersions and half-light radii of Milky Way dSphs to infer $\{r_{\text{max}}, v_{\text{max}}\}$ degeneracy curves, and used structural parameters $\{r_{\text{max}}, v_{\text{max}}\}$ of simulated DM subhaloes to break this degeneracy. This approach neglects orbital constraints available for Milky Way dSphs, and associates simulated DM haloes to Milky Way dSphs independently of their orbit or accretion history. In a follow-up contribution we will explore statistical methods to incorporate information on the distance measurements, radial velocities and proper motions into our fits in order to constrain the accretion history of Milky Way dSphs. Instead of associating Milky Way dSphs to simulated DM subhaloes of a single merger tree, we will use a probabilistic approach to model the distribution of structural and orbital properties of DM subhaloes in Milky Way-like haloes, as introduced in Peñarrubia (2018).

5.5 Comparison with other studies

On the low-mass end of inferred masses, for the Hercules dwarf, we find an enclosed mass of $M_{\text{est}}(< 1.8R_h)/M_{\odot} = 6.6^{+4.1}_{-3.0} \times 10^6$. To compare this value against the mass $M(< 0.3 \text{ kpc})/M_{\odot} = 1.9^{+1.1}_{-0.8} \times 10^6$ inferred by Adén et al. (2009), we use the general form of the virial mass estimator (equation 13) with $\mu(\lambda = 0.3 \text{ kpc}/R_h) \approx 2.7 \pm 0.7$ (see Fig. 3). This choice of λ is different from the minimum variance choice $\bar{\lambda} = 1.8$, hence the larger uncertainty on μ . Ignoring the systematic uncertainty, we find $M_{\text{est}}(< 0.3 \text{ kpc})/M_{\odot} = 5.0^{+3.2}_{-2.3} \times 10^6$. This value is larger than the one quoted by Adén et al. (2009), however, in contrast to the reported value, it was not derived under the assumption of isotropy and

a flat velocity dispersion profile, but instead is valid independently of the underlying anisotropy profile.

Strigari et al. (2008) and Wolf et al. (2010) discuss a single mass scale of $10^9 M_\odot$ for the total masses of all Milky Way dwarf galaxies, making use of cosmological mass-size relations for cuspy haloes to extrapolate the total mass from masses enclosed within 300 pc and the deprojected half-light radius, respectively. This mass scale is in agreement with the total masses we derive for Milky Way dSphs, with exceptions at the low-mass end: for Bootes (I) and Hercules we find masses of the order $10^7 M_\odot$.

Few studies have attempted to infer the total halo masses for individual Milky Way dSph galaxies, a recent contribution being the non-equilibrium N -body models by Ural et al. (2015) for the Carina dSph. They model the DM distribution of Carina separately under the assumption of cuspy ($\gamma = 1$) and cored ($\gamma = 0$) Dehnen (1993) profiles, i.e. $\alpha = 1, \beta = 4$ in equation 10. For the cuspy model, they find a total halo mass $z = 0$ of $4.0_{-2.4}^{+4.1} \times 10^8 M_\odot$. This result is consistent with the mass we find under the assumption of virial equilibrium, namely $3.8_{-3.5}^{+6.4} \times 10^8 M_\odot$. For the cored model, Ural et al. (2015) find a total mass of $3.5_{-2.3}^{+3.9} \times 10^8 M_\odot$. Our cored model for the Carina dSph is particularly poorly constrained (see right-hand panel of Fig. 10), and a large range of simulated haloes with masses spanning $1.2 \times 10^8 - 4.3 \times 10^{10} M_\odot$ result compatible with the observed kinematics. This shows an advantage of (non-equilibrium) N -body models tailored to reproduce current observables by taking into account the orbit and tidal evolution of the dwarf, however this approach is computationally expensive and requires a series of assumptions about the underlying host potential.

6 CONCLUSIONS AND SUMMARY

Mass estimators for pressure supported systems play an important role in constraining the distribution of dark matter (DM) on the scale of dwarf spheroidal galaxies (dSphs). Kinematic data for these systems is often limited to velocity dispersion measurements $\sigma_{\text{los}}(r)$ along the line of sight. The challenge lies in constructing an estimator which does not rely on strong assumptions about quantities inaccessible to observation. In this contribution, we construct an estimator for the mass enclosed within 1.8 multiples of the projected half-light radius R_h of the stellar tracer population. This estimator is based on the projected virial theorem and minimises the uncertainty on the inferred masses arising from our ignorance on (i) the central slope γ of the DM profile, as well as on (ii) how deeply embedded the stellar tracer population is within the DM halo (equation 13):

$$M_{\text{est}}(< 1.8 R_h) \approx 3.5 \times 1.8 R_h G^{-1} \langle \sigma_{\text{los}}^2 \rangle,$$

where by $\langle \sigma_{\text{los}}^2 \rangle = 2K$ we denote the luminosity-averaged squared line-of-sight velocity dispersion of the stellar tracer population. This mass estimator has been tailored to give accurate masses for tidally stripped dwarf galaxies, which follow density profiles that scale as $\rho \propto r^{-5}$ at large radii (Peñarrubia et al. 2009, 2010)

The use of the projected virial theorem has several advantages over Jeans' equations for the construction of mass estimators:

- Our method does not suffer from the mass - anisotropy degeneracy. Jeans' equations depend on information about the anisotropy of the velocity dispersion, parametrised by the function $\beta(r) \equiv 1 - \sigma_{\text{los}}^2(r)/\sigma_\perp^2(r)$, therefore requiring knowledge about the velocity dispersion component $\sigma_\perp(r)$ orthogonal to the line of sight. The form of $\beta(r)$ might be different for each stellar population, and could be more complicated than a simple monotonic

function of radius. Our ignorance of $\beta(r)$ gives rise to the infamous mass - anisotropy degeneracy. The projected virial theorem $2K_{\text{los}} + W_{\text{los}} = 0$ instead makes use of the luminosity-averaged squared line-of-sight velocity dispersion $\langle \sigma_{\text{los}}^2 \rangle = 2K$, accessible to observation.

- Systematic biases of inferred enclosed masses $M_{\text{est}}(< 1.8 R_h)$ and derived central slopes γ are straightforward to estimate: they follow directly from the assumptions on the DM and stellar density profiles, and do not rely on assumptions on the difficult to constrain form of $\beta(r)$.

- The average squared dispersion $\langle \sigma_{\text{los}}^2 \rangle$ is a sum over all stars and does not require data to be binned. It therefore can be robustly computed also for systems with a low number of stars - carefully modelling the uncertainties due to sample size as pointed out by Laporte et al. (2018).

However, the use of the virial theorem requires to specify a (family of) DM mass distributions, i.e. the estimated enclosed masses are model dependent. The bias of the derived masses is predominantly driven by how deeply embedded the stellar tracer is within the DM halo. For this reason, masses enclosed within multiples of the half-light can be determined fairly accurately, whereas the total halo mass is only weakly constrained from measurements of $\langle \sigma_{\text{los}}^2 \rangle$ and R_h alone (see Fig. 3 for $\lambda \gg 1$).

We have tested the mass estimator on a suite of N -body mocks extracted from controlled re-simulations of the Aquarius A2 merger tree (based on Errani et al. 2017), and recover the enclosed masses with an accuracy of $\lesssim 10$ per cent in systems with mass loss fractions that differ by orders of magnitude. The re-simulations cover all subhaloes of the merger tree with masses at infall $\geq 10^8 M_\odot$, and model each subhalo with the same number of 10^7 N -body particles independent of its mass. This set-up allows us to follow the tidal evolution of subhaloes spanning many orders of magnitude of mass and size, limiting numerical issues like artificial disruption of poorly-resolved low-mass substructures (see van den Bosch et al. 2018). Motivated by the mounting observational evidence of DM cores in Milky Way dwarfs (see e.g. Walker & Peñarrubia 2011; Amorisco et al. 2013), we run simulations assuming either cuspy or cored Dehnen (1993) DM density profiles for the subhaloes at infall. We apply the minimum variance mass estimator to a catalogue Milky Way dwarf galaxies (McConnachie 2012), showing a tight correlation between enclosed mass $M(< 1.8 R_h)$ and luminosity L_* . Using empirical functions (*tidal tracks*) fitted to the evolution of stellar tracers embedded in the DM subhaloes of our re-simulations of the Aquarius merger tree, we show that the correlation between enclosed mass and luminosity does not evolve significantly due to tidal stripping even when dwarfs lose more than one order of magnitude of their initial mass. Our results suggest that the currently observed correlation is mainly driven by internal processes such as star-formation and feedback. We furthermore find that the mean densities $\langle \rho(< 1.8 R_h) \rangle$ of ultra-faint galaxies are too high to be compatible with any of the simulated cored DM haloes, and show that tidal evolution further increases this discrepancy. This is a consequence of our choice of core size of the simulated DM haloes (a core size equal to the scale radius), and our findings suggest that the densities of ultra faint galaxies require core sizes that are much smaller than the scale radius of the DM halo.

Constraints on the total halo mass from measurements of $\langle \sigma_{\text{los}}^2 \rangle$ and R_h alone are weak given our ignorance on how deeply embedded the stellar population is within the DM halo. For 2-parameter DM density profiles - like the $\{\alpha, \beta, \gamma\} = \{1, 5, 0\}$ and $\{1, 5, 1\}$ profiles - the measurements of $\langle \sigma_{\text{los}}^2 \rangle$ and R_h however do

constrain the DM halo structural parameters $\{r_{\max}, v_{\max}\}$ to follow a one-dimensional degeneracy curve which can be cast as a function of the segregation parameter R_h/r_{\max} . Using our re-simulations of the Aquarius merger tree, we break this degeneracy by selecting those simulated DM subhaloes with $\{r_{\max}, v_{\max}\}$ values consistent with the degeneracy curve. This allows us to infer the total halo masses of Milky Way dwarf galaxies. We have tested this method using mocks generated from re-simulations of the Aquarius merger tree and show that total halo masses are robustly recovered within a factor of the order of unity for both cuspy and cored DM haloes. Our findings suggest that the classical Milky Way dSphs are embedded in haloes spanning a narrow range of masses, $8 < \lg(M/M_\odot) < 10$, with no clear trend with either galaxy size or luminosity. Surprisingly, we find that the stellar mass and halo mass of ultra-faint galaxies are *anti-correlated*, i.e. the halo mass *decreases* with increasing stellar mass. We caution that this anti-correlation may be caused by either observational inaccuracies (contamination by foreground stars, inflated velocity dispersions due to binary motion), or that the Aquarius A2 merger tree does not contain subhaloes representative of those of ultra-faints.

With velocity measurements becoming available also tangentially to the line of sight (e.g. [Massari et al. 2018](#)), note that it is straightforward to extend the virial mass estimator to systems with full kinematic information, as the spherical virial theorem reads (cf. equation 1):

$$\langle \sigma_{\text{los}}^2 \rangle + \langle \sigma_\alpha^2 \rangle + \langle \sigma_\delta^2 \rangle = 4\pi G \int_0^\infty r v_\star(r) M(< r) dr, \quad (26)$$

with $\langle \sigma_\alpha^2 \rangle$ and $\langle \sigma_\delta^2 \rangle$ denoting the luminosity-averaged squared velocity dispersions of the two velocity components tangential to the line of sight. Motivated by the new orbital constraints for Milky Way dSphs ([Gaia Collaboration et al. 2018](#)) and ultra-faints ([Simon 2018](#)) available thanks to the Gaia satellite, in a future contribution, we will study how to make use of orbital motion and internal kinematics to further constrain the properties of DM haloes of Milky Way dSphs and their accretion histories.

Acknowledgements

This work used the ARCHER UK National Supercomputing Service (<http://www.archer.ac.uk>), and the authors would like to thank the administrators for their support. We thank the VIRGO Consortium for giving us access to the Aquarius trees. RE acknowledges support through the Scottish University Physics Alliance.

References

Adén D., Wilkinson M. I., Read J. I., Feltzing S., Koch A., Gilmore G. F., Grebel E. K., Lundström I., 2009, *ApJ*, **706**, L150
 Agnello A., Evans N. W., 2012, *ApJ*, **754**, L39
 Amorisco N. C., Evans N. W., 2011, *MNRAS*, **411**, 2118
 Amorisco N. C., Evans N. W., 2012, *MNRAS*, **419**, 184
 Amorisco N. C., Agnello A., Evans N. W., 2013, *MNRAS*, **429**, L89
 Battaglia G., Helmi A., Tolstoy E., Irwin M., Hill V., Jablonka P., 2008, *ApJ*, **681**, L13
 Behroozi P. S., Wechsler R. H., Conroy C., 2013, *ApJ*, **770**, 57
 Binney J., Mamon G. A., 1982, *MNRAS*, **200**, 361
 Binney J., Tremaine S., 1987, Galactic dynamics
 Boylan-Kolchin M., Bullock J. S., Kaplinghat M., 2011, *MNRAS*, **415**, L40
 Breddels M. A., Helmi A., van den Bosch R. C. E., van de Ven G., Battaglia G., 2013, *MNRAS*, **433**, 3173
 Bullock J. S., Johnston K. V., 2005, *ApJ*, **635**, 931
 Bullock J. S., Kolatt T. S., Sigad Y., Somerville R. S., Kravtsov A. V., Klypin A. A., Primack J. R., Dekel A., 2001, *MNRAS*, **321**, 559
 Caldwell N., et al., 2017, *ApJ*, **839**, 20

Campbell D. J. R., et al., 2016, preprint, ([arXiv:1603.04443](https://arxiv.org/abs/1603.04443))
 Chan T. K., Kereš D., Oñorbe J., Hopkins P. F., Muratov A. L., Faucher-Giguère C.-A., Quataert E., 2015, *MNRAS*, **454**, 2981
 Dehnen W., 1993, *MNRAS*, **265**, 250
 Diakogiannis F. I., Lewis G. F., Ibata R. A., 2014, *MNRAS*, **443**, 598
 Errani R., Peñarrubia J., Tormen G., 2015, *MNRAS*, **449**, L46
 Errani R., Peñarrubia J., Laporte C. F. P., Gómez F. A., 2017, *MNRAS*, **465**, L59
 Fattahi A., Navarro J. F., Frenk C. S., Oman K. A., Sawala T., Schaller M., 2018, *MNRAS*, **476**, 3816
 Gaia Collaboration et al., 2018, preprint, ([arXiv:1804.09381](https://arxiv.org/abs/1804.09381))
 González-Samaniego A., Bullock J. S., Boylan-Kolchin M., Fitts A., Elbert O. D., Hopkins P. F., Kereš D., Faucher-Giguère C.-A., 2017, *MNRAS*, **472**, 4786
 Hopkins P. F., Kereš D., Oñorbe J., Faucher-Giguère C.-A., Quataert E., Murray N., Bullock J. S., 2014, *MNRAS*, **445**, 581
 Laporte C. F. P., Walker M. G., Peñarrubia J., 2013, *MNRAS*, **433**, L54
 Laporte C. F. P., Agnello A., Navarro J. F., 2018, preprint, ([arXiv:1804.04139](https://arxiv.org/abs/1804.04139))
 Lokas E. L., Mamon G. A., 2003, *MNRAS*, **343**, 401
 Lokas E. L., Kazantzidis S., Majewski S. R., Law D. R., Mayer L., Frinchaboy P. M., 2010, *ApJ*, **725**, 1516
 Martin N. F., de Jong J. T. A., Rix H.-W., 2008, *ApJ*, **684**, 1075
 Massari D., Breddels M. A., Helmi A., Posti L., Brown A. G. A., Tolstoy E., 2018, *Nature Astronomy*, **2**, 156
 McConnachie A. W., 2012, *AJ*, **144**, 4
 Merrifield M. R., Kent S. M., 1990, *AJ*, **99**, 1548
 Merritt D., 1987, *ApJ*, **313**, 121
 Miyamoto M., Nagai R., 1975, *PASJ*, **27**, 533
 Moster B. P., Somerville R. S., Maudsott C., van den Bosch F. C., Macciò A. V., Naab T., Oser L., 2010, *ApJ*, **710**, 903
 Navarro J. F., Frenk C. S., White S. D. M., 1997, *ApJ*, **490**, 493
 Peñarrubia J., 2018, *MNRAS*, **474**, 1482
 Peñarrubia J., McConnachie A. W., Navarro J. F., 2008a, *ApJ*, **672**, 904
 Peñarrubia J., Navarro J. F., McConnachie A. W., 2008b, *ApJ*, **673**, 226
 Peñarrubia J., Navarro J. F., McConnachie A. W., Martin N. F., 2009, *ApJ*, **698**, 222
 Peñarrubia J., Benson A. J., Walker M. G., Gilmore G., McConnachie A. W., Mayer L., 2010, *MNRAS*, **406**, 1290
 Peñarrubia J., Gómez F. A., Besla G., Erkal D., Ma Y.-Z., 2016, *MNRAS*, **456**, L54
 Prada F., Klypin A. A., Cuesta A. J., Betancort-Rijo J. E., Primack J., 2012, *MNRAS*, **423**, 3018
 Read J. I., Steger P., 2017, *MNRAS*, **471**, 4541
 Richardson T., Fairbairn M., 2014, *MNRAS*, **441**, 1584
 Saglia R. P., Kronawitter A., Gerhard O., Bender R., 2000, *AJ*, **119**, 153
 Sanders J. L., Evans N. W., Dehnen W., 2018, preprint, ([arXiv:1802.09537](https://arxiv.org/abs/1802.09537))
 Sawala T., et al., 2015, *MNRAS*, **448**, 2941
 Sawala T., et al., 2016, *MNRAS*, **457**, 1931
 Simon J. D., 2018, preprint, ([arXiv:1804.10230](https://arxiv.org/abs/1804.10230))
 Springel V., et al., 2008, *MNRAS*, **391**, 1685
 Strigari L. E., Bullock J. S., Kaplinghat M., 2007, *ApJ*, **657**, L1
 Strigari L. E., Bullock J. S., Kaplinghat M., Simon J. D., Geha M., Willman B., Walker M. G., 2008, *Nature*, **454**, 1096
 Torrealba G., Kopev S. E., Belokurov V., Irwin M., 2016, *MNRAS*, **459**, 2370
 Ural U., Wilkinson M. I., Read J. I., Walker M. G., 2015, *Nature Communications*, **6**, 7599
 Walker M. G., Peñarrubia J., 2011, *ApJ*, **742**, 20
 Walker M. G., Mateo M., Olszewski E. W., Gnedin O. Y., Wang X., Sen B., Woodroffe M., 2007, *ApJ*, **667**, L53
 Walker M. G., Mateo M., Olszewski E. W., Peñarrubia J., Wyn Evans N., Gilmore G., 2009, *ApJ*, **704**, 1274
 Wang W., Han J., Cooper A. P., Cole S., Frenk C., Lowing B., 2015, *MNRAS*, **453**, 377
 Watkins L. L., van de Ven G., den Brok M., van den Bosch R. C. E., 2013, *MNRAS*, **436**, 2598

Wolf J., Martinez G. D., Bullock J. S., Kaplinghat M., Geha M., Muñoz R. R., Simon J. D., Avedo F. F., 2010, *MNRAS*, 406, 1220
 de Boer T. J. L., et al., 2012, *A&A*, 544, A73
 van den Bosch F. C., Ogiya G., Hahn O., Burkert A., 2018, *MNRAS*, 474, 3043

APPENDIX A: TIDAL EVOLUTIONARY TRACKS

Structural parameters of dwarf galaxies that are being tidally stripped can be parametrised as simple analytical functions which depend only on the total fraction of mass lost, but not on the specific orbit of the dwarf, or the host potential. This has been first discussed by Peñarrubia et al. (2008b) for the case of spherical stellar systems embedded in cuspy DM haloes, who named these analytical functions *tidal evolutionary tracks*. Similarly, Errani et al. (2015) discuss tidal tracks for spherical dwarf galaxies with cored DM haloes, whereas Sanders et al. (2018) study dwarf galaxies where both the stellar tracer and the DM halo are flattened. In the following, we derive such tracks for DM subhaloes and dwarf galaxies in the re-simulations of the Aquarius A2 merger tree discussed in section 3.2. In contrast to the tracks of Peñarrubia et al. (2008b), instead of fitting the evolution of single galaxies on different orbits at subsequent apocentres, we fit tracks to the entire population of simulated dwarf galaxies at $z = 0$. We fit the DM halo radius of maximum circular velocity r_{\max} , the total stellar mass of the embedded stellar population M_* and the half-light radius R_h , normalised by their initial values (i.e. at z_{infall}), as functions of the remnant mass M_{\max} enclosed within r_{\max} . This parametrisation is motivated by the fact that the enclosed mass M_{\max} can be measured directly from the N -body snapshots of the simulation, without having to assume a specific mass profile. For the fits, we adapt the empirical formula of Peñarrubia et al. (2008b) introducing as third parameter the scale x_s :

$$g(x) = \frac{(1+x_s)^\alpha x^\beta}{(x+x_s)^\alpha} \quad \text{with} \quad x = M_{\max}/M_{\max,0}, \quad (\text{A1})$$

where $g(x) = r_{\max}(x)/r_{\max,0}$, $M_*(x)/M_{*,0}$ or $R_h(x)/R_{h,0}$, respectively. We introduce the scale x_s to use the same parametrisation $x = M_{\max}/M_{\max,0}$ for both the DM- and the stellar tracks: the choice of $x_s = 1$ in the formula of Peñarrubia et al. (2008b) was adapted for tidal tracks parametrised by mass lost within the initial half-light radius, but does not yield reasonable fits for structural parameters of the stellar population when expressing the tidal tracks as functions of $x = M_{\max}/M_{\max,0}$. We do not fit the scale parameter x_s , but where the functional shape of $g(x)$ requires it, we use as scale the initial fraction of mass enclosed within the initial half-light radius: $x_s = (1 + a_0/R_{h,0})^{\gamma-3}$, where by a_0 we denote the initial Dehnen (1993) scale radius of the halo. This choice reduces the dependence of the fits on segregation, and motivated the choice of $x_s = 1$ in the stellar tracks derived by Peñarrubia et al. (2008b). We fit tidal tracks separately for cuspy ($\gamma = 1$) and cored ($\gamma = 0$) dwarf galaxies which at z_{infall} had Dehnen (1993) density profiles, i.e. $\{\alpha, \beta, \gamma\} = \{1, 4, \gamma\}$. Fits are done separately for two stellar populations with initial segregations of $R_{h,0}/r_{\max,0} = 1/20$ and $1/10$. To limit the impact of numerical artefacts caused by the spatial resolution of the particle mesh code, the highest-resolving co-moving grid having a spacing of $r_{\max,0}/128$, we include only haloes in the fits with $r_{\max}/r_{\max,0} > 1/10$. We only consider bound N -body particles for the fits, and fit only haloes where both the DM and the stellar tracer are approximately in virial equilibrium, requiring that $|2K + W|/(2K - W) < 0.2$ for the DM enclosed within r_{\max} , and $|2K_{\text{los}} + W_{\text{los}}|/(2K_{\text{los}} - W_{\text{los}}) < 0.05$ for the stars. Halo properties are then averaged in logarithmically spaced bins spanning $0.01 \leq M_{\max}/M_{\max,0} \leq 1$ to avoid giving different weight to various mass fractions based on the halo abundance at that mass fraction. The empirical fit parameters are listed in table A1. Fig. A1 shows the fitted tidal tracks, as well as the parameters of single dwarf galaxies at $z = 0$ used for the fit. Note that r_{\max} of cored dwarf galaxies decreases less rapidly during tidal stripping than for their cuspy counterparts, and half-light radii of stellar populations embedded in cored DM haloes expand during tidal stripping.

This paper has been typeset from a $\text{\TeX}/\text{\LaTeX}$ file prepared by the author.

Table A1. Empirical fit parameters for equation A1. By $r_{\max,0} \equiv r_{\max}/r_{\max,0}$ we denote the radius of maximum circular velocity of the DM halo at $z = 0$, normalised by its initial value. Similarly, $M_{*,0} \equiv M_*/M_{*,0}$ and $R_{h,0} \equiv R_h/R_{h,0}$ are the total stellar mass and half-light radius of stellar populations embedded inside the DM halo, normalised by their respective initial value. We separately list parameters for two stellar populations with initial segregations of $R_{h,0}/r_{\max,0} = 1/20$ and $1/10$.

	$R_{h,0}/r_{\max,0}$	CUSP			CORE		
		α	β	$\lg x_s$	α	β	$\lg x_s$
$r_{\max,0}$	–	0.00	0.48	0.00	-0.85	0.00	0.00
$M_{*,0}$	1/20	1.87	1.87	-2.64	2.83	2.83	-3.12
	1/10	1.80	1.80	-2.08	2.05	2.05	-2.33
$R_{h,0}$	1/20	0.47	0.41	-2.64	-0.25	-0.25	0.00
	1/10	0.50	0.42	-2.08	-0.23	-0.23	0.00

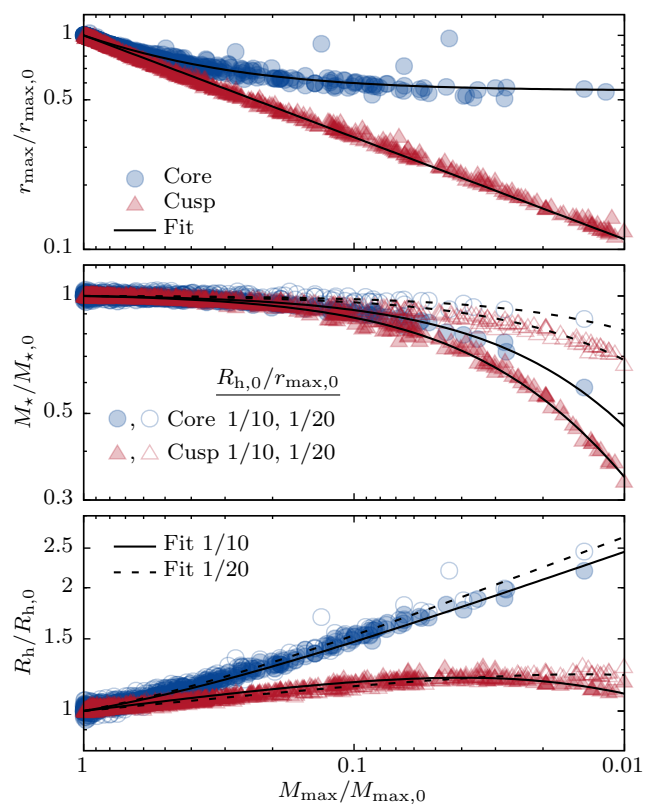


Figure A1. Structural properties of dwarf galaxies are simple functions of the remnant bound mass only. The top panel shows r_{\max} of the underlying DM halo, normalised by its initial value $r_{\max,0}$, as a function of the mass $M_{\max}/M_{\max,0}$ enclosed within r_{\max} . The evolution of r_{\max} is shown separately for cuspy (red triangles) and cored (blue circles) DM profiles. The central and bottom panel show the evolution of the central surface brightness and half-light radii of stellar populations embedded inside the DM haloes with initial segregation of $R_{h,0}/r_{\max,0} = 1/10$ (filled symbols), $1/20$ (open symbols).